DR 21738
MAY 2001
ISSUE 1

Utilisation of Pulsed Laser for SEE Testing

Study at Two Wavelengths

Report reference: ESA_QCA010801S_C

Prepared by .....
R Jones,
Principal Engineer

.....
A M Chugg,
Senior Principal Engineer

Approved by .....
A M Chugg,
Senior Principal Engineer

Authorised by .....
P Jones,
DDH Electronic Technology

European Space Agency Contract Report

The work described in this report was done under ESA contract
No. 13528/99/NL/MV, COO-03.
Responsibility for the contents resides in the author or organization that prepared it

ESTEC Technical Officer: R. Harboe-Sorensen

DR 21738
MAY 2001
ISSUE 1

Utilisation of Pulsed Laser for SEE Testing

Study at Two Wavelengths

ABSTRACT

This document describes a study aimed at investigating the utility of focussed picosecond laser pulses for Single Event Effect (SEE) testing of microcircuits. This study has concentrated principally upon the benefits of using different laser wavelengths for the testing of microcircuits, especially with regard to reducing feature sizes. The use of laser SEE test results over a range of wavelengths to probe the SEE sensitivity profile of memory cells with depth into the silicon has been invented and pioneered in this work. An important initial implication of this work has been that the sensitive thickness appears to be of the order of 10μm for all the samples and almost independent of feature size.

An initial investigation has also been undertaken into the utility of the laser system for relating output errors to specific SEE sensitive locations in programmable logic devices, ASIC's, microprocessors etc. An Actel FPGA has been programmed with a suitable circuit and tested with the laser system.

(A parallel study by Hirex has investigated the feasibility of laser pulsing from the rear of microchip dies in order to evade interference from metallisation layers, but this is reported elsewhere.)

This study has been undertaken as specified in the Matra BAe Dynamics (MBD) Statement of Work on the Utilisation of Pulsed Lasers for SEE Testing (ref. ED 13099) in conformance with the in the Hirex-MBD proposal to the ESA (ref. HRX/99.4770) by the Radiation Effects Group of Matra BAe Dynamics on behalf of the European Space Agency (ESA) under Contract No. 13528/99/NL/MV.

DOCUMENT CHANGE RECORD

DATE	NATURE OF CHANGE	IMPLEMENTER

Utilisation of Pulsed Laser for SEE Testing

Study at Two Wavelengths

CONTENTS

1.0 INTRODUCTION

1.1 Purpose Of This Document
1.2 Overview

2.0 CALIBRATED LASER TESTING OF SRAM'S

2.1 Introduction
2.2 Device Selection
2.3 Ion Beam Calibration
2.4 Infra-Red Laser Testing
2.5 Green Laser Testing
2.6 Comparison of Infrared and Green Results
2.7 Reflected Laser Pulse Energy

3.0 LASER MEASUREMENT OF MICROCHIP SENSITIVITY PROFILES

3.1 Introduction
3.2 Theory
3.3 Generalisation of the Technique
3.4 Analysis of Measurements
3.5 Advantages of the Laser Technique
3.6 Metallisation Interference and Measurement of Reflectance

4.0 LASER TESTING OF AN FPGA

4.1 Introduction
4.2 Device Selection and Test Circuit Design
4.3 Laser Testing

5.0 CONCLUSIONS AND RECOMMENDATIONS

5.1 Conclusions
5.2 Recommendations

REFERENCES

DISTRIBUTION

Utilisation of Pulsed Laser for SEE Testing
Study at Two Wavelengths

1.0 INTRODUCTION

1.1 Purpose Of This Document

1.1.1 This document constitutes the MBD Final Report for the European Space Agency's research project on Utilisation of Pulsed Lasers for SEE Testing in conformance with the work description in Section 1.4.2 of the Hirex-MBD proposal to the ESA (ref. HRX/99.4770). This work has been performed under ESA Contract No. 13528/99/NL/MV.

1.2 Overview

1.2.1 This report is an account of empirical laser SEE studies at two wavelengths upon a wide range of 1Mbit SRAM's and upon an FPGA. SRAM's were selected from three different manufacturers. For each manufacturer the same device was purchased in several different feature sizes, giving a total of nine die designs for testing. The intention was to study the relative performance of green (532nm) and infrared (1064nm) laser pulses and to investigate whether the reduced spot size of the green pulses might provide improved performance for the smaller feature sizes in the ranges.

1.2.2 It has also been noted that the generation of laser pulse upset threshold energies at a range of different wavelengths can be used to investigate the depthwise sensitivity profile of microelectronic devices to radiation delivered charge. A section of this report therefore describes the theoretical basis of this novel technique in mathematical detail and the implications of the green:infrared upset threshold ratios established in this work for the sensitive thickness of the SRAM devices have been analysed.

1.2.3 The FPGA testing was designed to investigate the utility of the laser as a tool for relating output errors induced by SEE's to specific sensitive locations and circuit elements on the FPGA die. The problem has been that the induced errors in circuit elements are fed through the intervening FPGA circuitry before being manifested at the outputs and they are considerably modified in the process. It is therefore difficult to attribute a given output error to a given circuit element upset in these types of devices, unless the position of the induced error on the die surface is known. Laser investigations, which provide the location information, are therefore potentially useful in producing SEE resistant FPGA and ASIC designs and also in validating some modelling approaches, which have been employed to seek to relate element upsets to the corresponding output error distributions. An Actel 54SX16 FPGA was selected for this investigation. Output errors were successfully related to laser pulsing at specific die locations and the sensitive locations were found to be small and few for this device.

1.2.4 The laser system, which has been used to conduct these investigations, is outlined in

Figure 1.1. It was inaugurated at the end of 1998 and is known as the Single Event Radiation Effects in Electronics Laser (SEREEL) facility. It currently delivers 40picosecond laser pulses of up to 30mJ energy at up to 10Hz at 1064nm and 532nm wavelengths, the latter having been added in a system upgrade during the course of these studies. The pulse energy is continuously adjustable by means of neutral density filters and crossed-polarisers. Samples of the attenuated beam are taken with PIN diodes and photodiodes, so as to measure the delivered pulse energy. The pulses are brought to a diffraction limited focus with a spot diameter fractionally larger than the wavelength by passing them down a microscope from the eyepiece end to the objective. A delidded microcircuit can be positioned and repositioned by three-axis nanostep positioners under computer control so as to deliver large arrays of laser spots across its die surface.

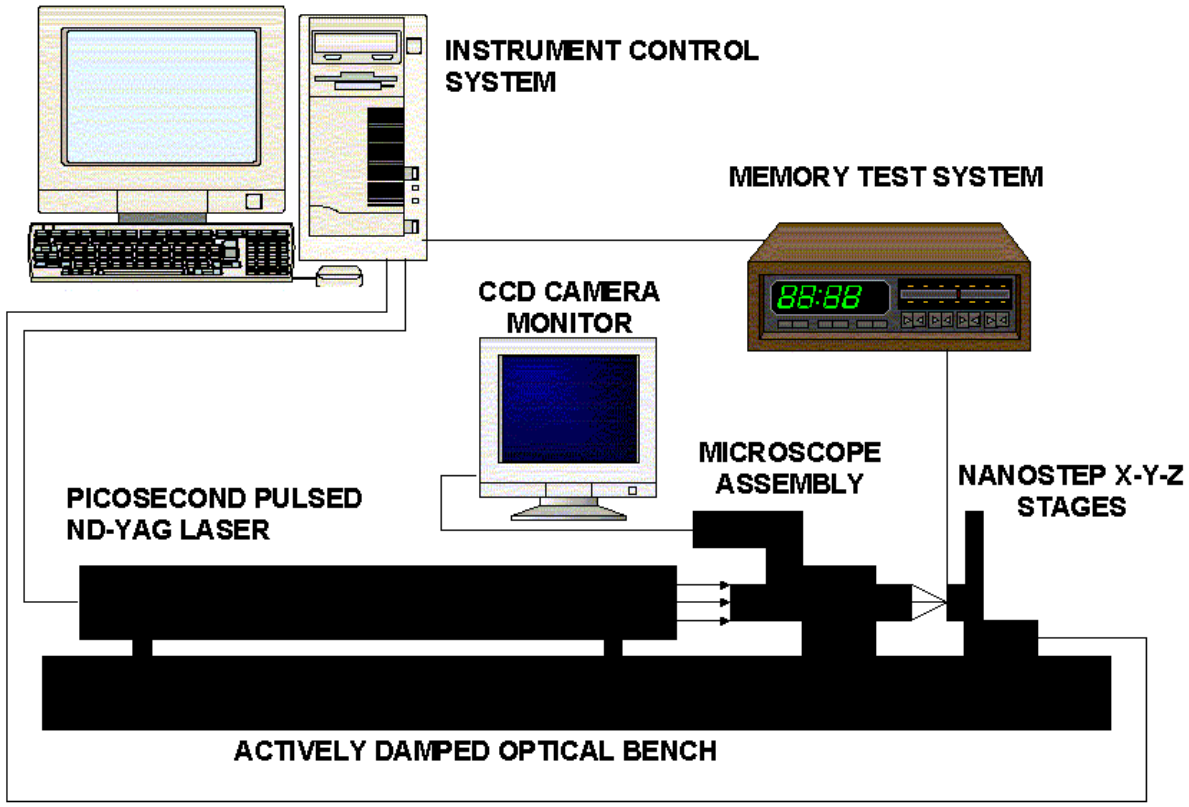

Figure 1.1. The SEREEL picosecond pulsed laser facility.

2.0 CALIBRATED LASER TESTING OF SRAM'S

2.1 Introduction

2.1.1 The testing has been aimed in the first instance at establishing the variation in the performance of laser pulse testing calibrated against ion test results according to variation of:-

a) Laser pulse wavelength

b) Device feature size

To this end laser testing has been performed at both green (0.532μm) and infra-red (1.06μm) wavelengths for sets of memory chips from the same manufacturers spanning ranges of feature size between 0.3μm and 0.8μm.

2.1.2 Samples of the chosen devices have been delidded and upset cross-section curves have been generated for each device at both wavelengths and compared with ion test curves obtained at the UCL cyclotron HIF.

2.2 Device Selection

2.2.1 In consultation with ESA it was decided that 3 device types should be included in the investigation of the variations in the laser performance with feature size and laser pulse wavelength.

2.2.2 The preferred parts were 4Mbit SRAM's, but it was discovered that a sufficient spread of feature size is not generally available in 4Mbit parts, mainly because they do not exist in the larger feature sizes. Furthermore, it was difficult to obtain 4Mbit parts even in a narrow range of feature sizes, because at the time of ordering in March 2000 production had largely been assigned to mobile phone companies until around October 2000. Consequently, the study has proceeded on the basis of 1Mbit SRAM samples. The selected types are listed in Table 2.1.

Device type	Feature sizes
Cypress CY7C109	0.65, 0.5 and 0.42 micron
Mitsubishi M5M51008	0.8, 0.6 and 0.4 micron
Samsung KM681000	0.7, 0.6, 0.4 and 0.3 micron

Table 2.1. Selected 1Mbit SRAM parts for the laser SEE study.

2.2.3 10 samples of each type at each feature size were purchased. They were delidded at the Matra BAe Dynamics facility in Velizy, Paris. Two or three samples were consumed in setting up the process. Five samples of each feature size were delidded, leaving two or three spare for emergencies and as controls. Of the delidded samples around 50% manifested some degree of functional failure, so only two or three samples were typically available for testing. In addition, one or two device samples of each type (either undelidded or delidded, but with a functional failure) were subsequently forwarded to ESTEC for constructional analysis by the NMRC

laboratory in Ireland.

2.2.4 A problem was identified during microscope inspection of the bare dies. The Cypress devices, which the supplier had claimed were in 0.5 micron feature size, appeared to have identical dies to the 0.65 micron devices.

2.3 Ion Beam Calibration

2.3.1 Ion beam SEE testing of all the SRAM types was conducted in November 2000 at the CYCLONE facility at UCL. The test board (with 18 delidded samples) is shown mounted in the (open) CYCLONE vacuum irradiation chamber in Figure 2.1. A detailed view of the test board showing the two rows of test samples is given in Figure 2.2. A PC was used to detect errors in an initial "checkerboard" pattern of ones and zeroes loaded into the memories. Accurate LET cross-section curves were obtained for two samples of each device type except for the Samsung parts of type A and E, where results were only obtained for a single sample. Ion cocktail number 1 was used throughout this testing. This comprises Xenon-132, Krypton-84, Argon-40, Neon-20, Nitrogen-15 and Boron-10 ions with LET's of 55.5, 34, 14.1, 5.85, 2.97 and 1.7 MeV/(mg/cm^2) at normal incidence. Intermediate LET's were obtained by inclining the test board to give incidence angles of up to 60 degrees.

2.3.2 The results are shown in Figures 2.3 to 2.11 and some summary data are given in Table 2.2. These graphs are generally very nice with well-defined upset thresholds and saturation cross-sections. The thresholds ranged between 1.4 and 4.5 MeV/(mg/cm^2), whilst the saturation cross-sections varied between 2E-8 and 7E-7 cm^2/bit. These results provide a very good basis for laser pulse energy calibration against LET.

2.4 Infra-Red Laser Testing

2.4.1 The MBD Single Event Radiation Effects in Electronics Laser facility (SEREEL) was used to deliver arrays of laser pulses across the entire exposed surfaces of the delidded SRAM samples. Typically at least 1600 laser pulses were delivered to each sample at each laser pulse energy. However, this number was sometimes increased to 3000 or more at pulse energies where very few errors were recorded in order to improve the statistical accuracy of the results. In general there is a standard error or uncertainty on the number of errors N_E of $\sqrt{N_E}$. It may be noted with reference to Figure 2.12 that the absorption length for 1064nm infrared pulses in silicon is about 0.5mm, so these pulse are not significantly attenuated on the thickness scale of a memory cell.

2.4.2 The resulting laser cross-section curves have been fitted to the corresponding ion cross-sections as shown in Figures 2.13 to 2.17. In general the laser cross-section values are more uncertain at the lower cross-section values, because of the $\sqrt{N_E}$ error. Conversely, the fit cannot rely on points in or near the saturation region, because the slopes are too flat to give good accuracy. The fitting has therefore concentrated on achieving good agreement in the intermediate range of cross-sections (circa 1E-9 to 1E-8 cm^2 per bit). A further guiding principle is the fact that almost all calibration errors, laser focussing errors etc. tend to give relatively larger pulse energies for a given cross-section value: it is therefore reasonable to assume that the lowest values

of pulse energy for a given cross-section are the most reliable.

2.4.3 The calibration factors derived from these curve fits are given in Table 2.2. They lie in the range 0.077 to 0.417 nJ per MeV/(mg/cm^2) with a mean of 0.22nJ per MeV/(mg/cm^2) and a standard deviation of 0.13 nJ per MeV/(mg/cm^2).

2.4.4 Latchups were seen for several samples at higher pulse energies than the upset threshold, but latchups were seen at 0.8nJ for the Mitsubishi M5M51008B, before any upsets had been recorded. In the case of the Cypress CY7C109 at 0.65μm feature size latchups were seen with ions and with infrared laser pulses, but the laser threshold was about 60% lower relative to the upset threshold. It is normal for latchup to be easier with infrared laser pulses than with ions, possibly due to the fact that infrared is very efficient at delivering ionisation to the deep substrate.

2.5 Green Laser Testing

2.5.1 1-10 picosecond pulsed Neodymium-YAG laser has a normal operating wavelength of 1.064 micrometres. However, an option exists to adapt the output using frequency doubling, tripling or quadrupling devices. These are used in conjunction with the appropriate wavelength separation package (WSP). The dichroic mirrors are mounted on rotatable platforms and can be set in one of two positions depending on the desired output wavelength.

2.5.2 Frequency doubling is achieved using a type II KD*P crystal mounted on an HP-02 mechanical holder. The crystal is oriented along a vertical plane by the large thumbwheel accessible from outside the laser cover. With the WSP in the appropriate configuration the 532nm energy output through port 2 is measured. The toggle switch on the side of the laser is then adjusted to maximise the pulse energy. It is necessary to be diligent in the performance of this tuning operation, since there are several side maxima. In addition the 1064nm input polarisation needs to be optimised by adjusting the λ/4plates located prior to the amplifier unit. By this means the laser was successfully modified to provide visible green pulses in addition to the standard infra red output in July 2000. The diffraction limit on the spot size is approximately equal to the wavelength, so 532nm spots are potentially half the diameter of 1064nm pulses. Furthermore, the absorption length (Figure 2.12) is about 1μm at 532nm, so green pulses are strongly attenuated on the depth scale of memory cells.

2.5.3 The 1Mbit SRAM samples were tested using green laser pulses in the same fashion as with infrared pulses. The results have been fitted to the corresponding ion cross-sections as shown in Figures 2.18 to 2.25. The corresponding calibration factors are given in Table 2.2. They lie in the range 6.67 to 20 pJ per MeV/(mg/cm^2) with a mean of 9.8pJ per MeV/(mg/cm^2) and a standard deviation of 4.3 pJ per MeV/(mg/cm^2).

2.6 Comparison of Infrared and Green Results

2.6.1 The fitted calibration coefficients for the SRAM devices have been plotted against their feature sizes for infrared and green laser testing in Figures 2.26 and 2.27 respectively. There is little evidence for any significant variations in the calibration coefficients with feature size. The best fit trends to these data would show a slight

increase in the calibration coefficients with reducing feature size, but this trends are very weak. For the green results in particular the flatness of the trend is surprising and probably significant, for it implies that the sensitive thickness of the memory cells is not scaling down with feature size for SRAM's in this feature size range. If the sensitive thickness were scaling with feature size, then the calibration coefficient at 532nm should be approximately linearly proportional to feature size.

2.6.2 It is notable that the green results are better correlated with one another than the infrared coefficients. It may also be added that visible pulses are much easier to work with from a practical point of view and that the problem of relatively low latchup thresholds experienced in infrared testing is much alleviated for green pulses. Furthermore, the green spot size is better and produces an ionisation column which is more representative of that generated by an ion. The only deficiency of green pulses is their rapid attenuation with depth, but this is not too serious if the sensitive thickness begins at the optical surface of the die. In general, the results of this testing show that green lasers pulses (and probably visible range pulses at higher wavelengths - orange and red) are superior to infrared pulses for SEE testing.

2.7 Reflected Laser Pulse Energy

2.7.1 Laser pulse energy is both absorbed and reflected at the microchip surface. It is desirable to calculate the proportion which is reflected in order to relate the laser pulse effects more directly to the amount of laser energy deposited in the silicon. One approach is to calculate an equivalent Linear Energy Transfer (LET) for the laser pulses and to relate this to the ion beam threshold LET for upset. An effective equivalent LET for a laser pulse of absorbed energy E_{abs} at depth x in silicon of absorptivity $f(\lambda)$ and density ρ is given by:-

$$\frac{1}{r}\frac{dE}{dx} = f(l)E_{abs}\exp(-f(l)x)/r$$

The silicon absorptivity $f(\lambda)$ is plotted in Figure 2.12. Its value is about $20cm^{-1}$ at 1064nm and about $1E4cm^{-1}$ at 532nm. This gives an absorption length of 500μm in the infrared, but only 1μm in the green. In the infrared it is therefore a reasonable approximation to equate the surface value (x=0) of the laser pulse Linear Energy Transfer with the threshold ion LET (but the laser LET varies too rapidly with depth for this to be true at 532nm). This suggests a theoretical calibration constant of around 20pJ per MeV $mg^{-1}cm^2$ in the infra red, whereas the observed value is typically around 100pJ per MeV $mg^{-1}cm^2$. It unlikely that all of the difference is attributable to reflection losses, since this would imply that 80% of incident energy is typically being reflected and there are some other possible reasons for the discrepancy. Nevertheless, this tends to support CCD camera observations (comparing reflections with the reflectivity from metallisation, which is near 100%) that of the order of 50% of incident energy is being reflected for both green and infrared pulses.

2.7.2 It is clear that a quantitative pulse by pulse measure of the reflected energy is highly desirable in order to remove the uncertainties associated with the surface reflectance of microchips. In fact there is a straightforward means to achieve this. The CCD camera images of the laser spot could be captured with a framegrabber card and the pixel intensities in the region of the spot could be integrated to provide a direct self-

consistent measurement of reflected pulse energy. This could then be compared with the near 100% reflected spots, when the beam is focussed onto areas of metallisation. It is a strong recommendation of this work that such measurement system should be established for future work.

Part No	Manufacturer & Feature Size	Radiation Type	Calibration Fit or Ion Threshold @c.1E-9cm^2/bit	Saturation Threshold (cm²/bit)	Latch-up	Threshold energy ratio 1064:532nm
CY7C109	Cypress 0.65µm	Laser (532nm)	12.5 pJ/MeVcm^{2}mg^{-1}	?		26.67
		Laser (1064nm)	0.333 nJ/MeVcm^{2}mg^{-1}	3.00E-07	1.75nJ	
		Ion Beam	1.4MeVcm^{2}mg^{-1}	2.00E-07	11.8-14 MeVcm^{2}mg^{-1}	
CY7C109	Cypress 0.42µm	Laser (532nm)	7 pJ/MeVcm^{2}mg^{-1}	?		
		Laser (1064nm)	No upsets to 2.5nJ	No upsets to 2.5nJ		
		Ion Beam	4.5MeVcm^{2}mg^{-1}	2.00E-08	LET 11.8-14 MeVcm^{2}mg^{-1}	
M5M51008A	Mitsubishi 0.8µm	Laser (532nm)	6 pJ/MeVcm^{2}mg^{-1}	~1E-7		
		Laser (1064nm)	Not Tested	Not Tested		
		Ion Beam	4MeVcm^{2}mg^{-1}	1.00E-07		
M5M51008B	Mitsubishi 0.6µm	Laser (532nm)	10 pJ/MeVcm^{2}mg^{-1}	?		
		Laser (1064nm)	Latch-up	Latch-up	0.8-0.85nJ	
		Ion Beam	3.5MeVcm^{2}mg^{-1}	1.5E-07		
M5M51008C	Mitsubishi 0.4µm	Laser (532nm)	8 pJ/MeVcm^{2}mg^{-1}	?		20.83
		Laser (1064nm)	0.167 nJ/MeVcm^{2}mg^{-1}	?		
		Ion Beam	2MeVcm^{2}mg^{-1}	3.00E-08		
KM681000A	Samsung 0.7µm	Laser (532nm)	6.67 pJ/MeVcm^{2}mg^{-1}	5.00E-07		14.99
		Laser (1064nm)	0.1 nJ/MeVcm^{2}mg^{-1}	3.00E-07		
		Ion Beam	2.5MeVcm^{2}mg^{-1}	7.00E-07		
KM681000B	Samsung 0.6µm	Laser (532nm)	8 pJ/MeVcm^{2}mg^{-1}	?		9.62
		Laser (1064nm)	0.077 nJ/MeVcm^{2}mg^{-1}	~2E-7		
		Ion Beam	2MeVcm^{2}mg^{-1}	2E-07		
KM681000C	Samsung 0.4µm	Laser (532nm)	Not Tested	Not Tested		
		Laser (1064nm)	0.417 nJ/MeVcm^{2}mg^{-1}	?		
		Ion Beam	2.5MeVcm^{2}mg^{-1}	1E-07		
KM681000E	Samsung 0.3µm(TFT)	Laser (532nm)	20 pJ/MeVcm^{2}mg^{-1}	?		
		Laser (1064nm)	Not Tested	Not Tested		
		Ion Beam	2MeVcm^{2}mg^{-1}	2E-07		

Table 2.2. Summary of SRAM test results.

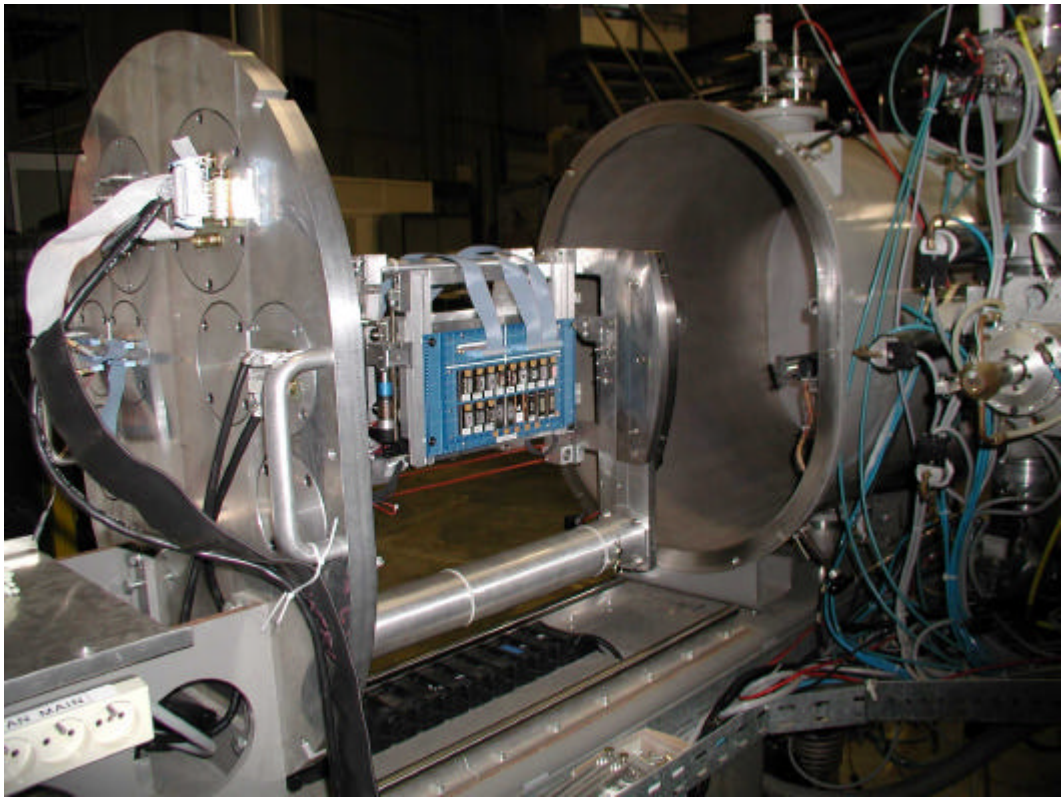

Figure 2.1. SRAM test board mounted in the UCL CYCLONE ion beam facility.

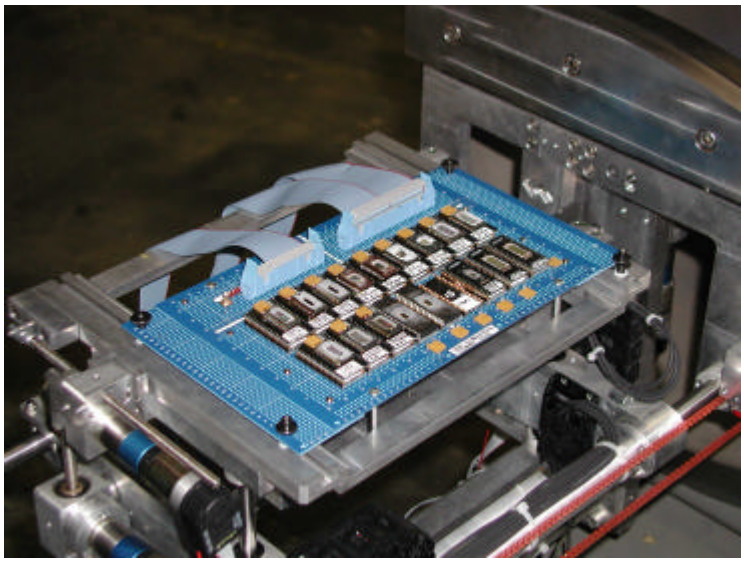

Figure 2.2. Delidded test samples on the SRAM test board at CYCLONE.

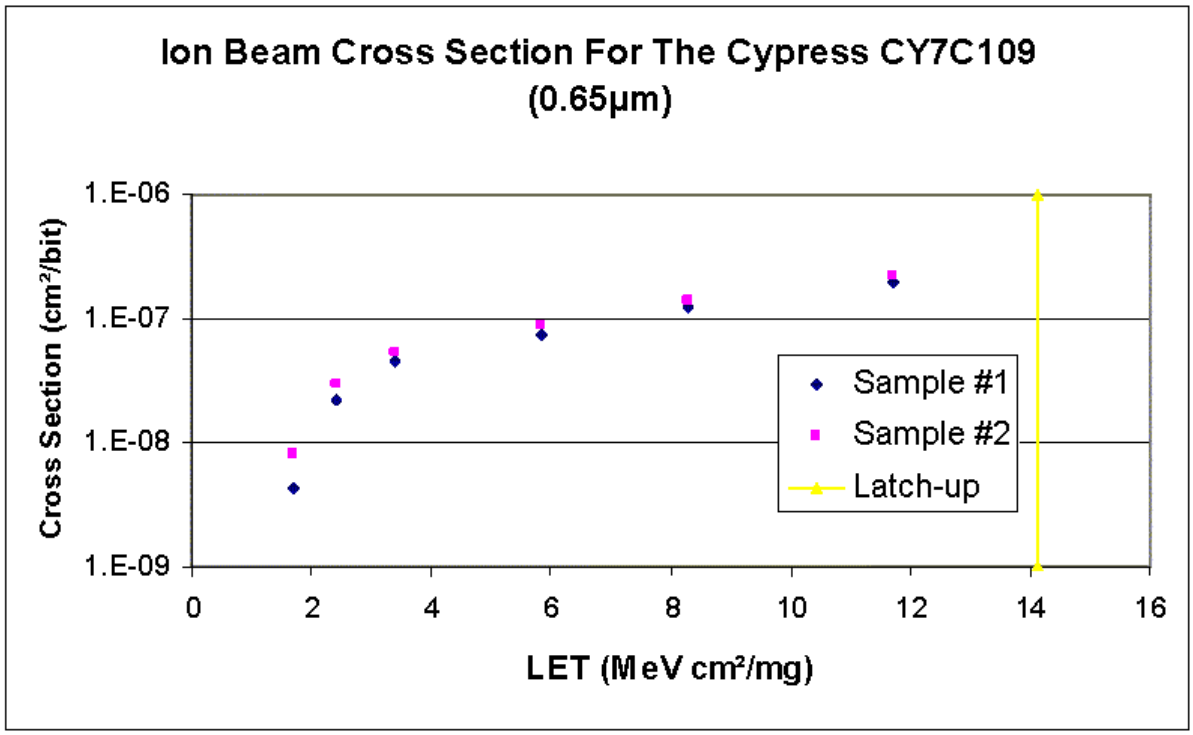

Figure 2.3. Ion beam cross section for the Cypress CY7C109 (0.65µm)

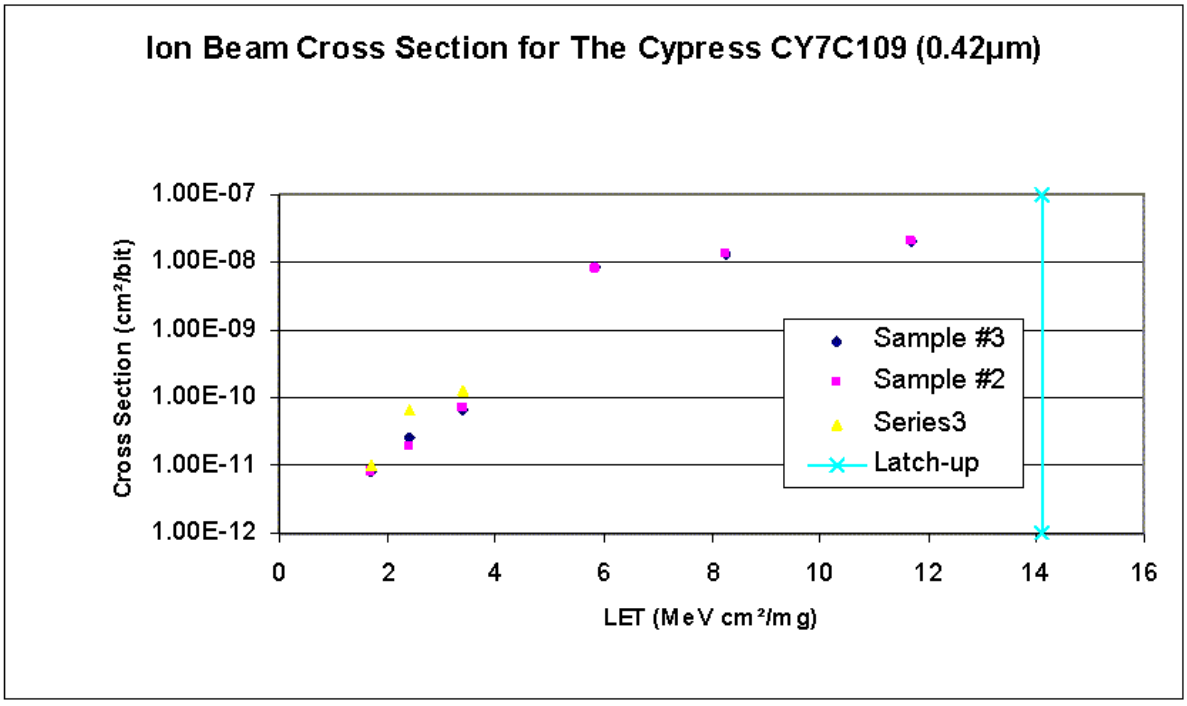

Figure 2.4. Ion beam cross section for the Cypress CY7C109 (0.42µm)

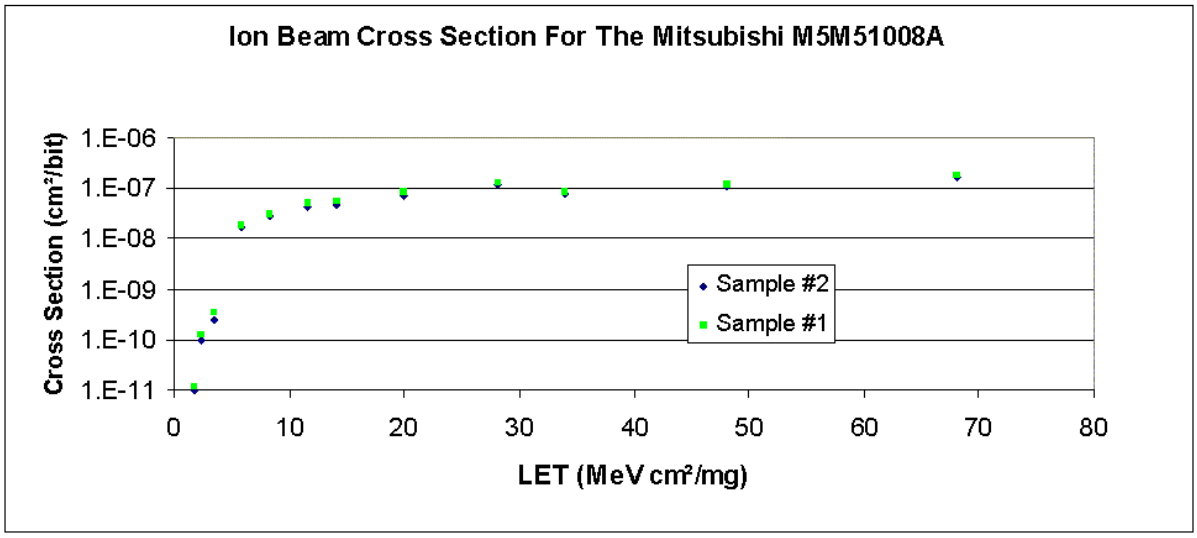

Figure 2.5. Ion beam cross section for the Mitsubishi M5M51008A

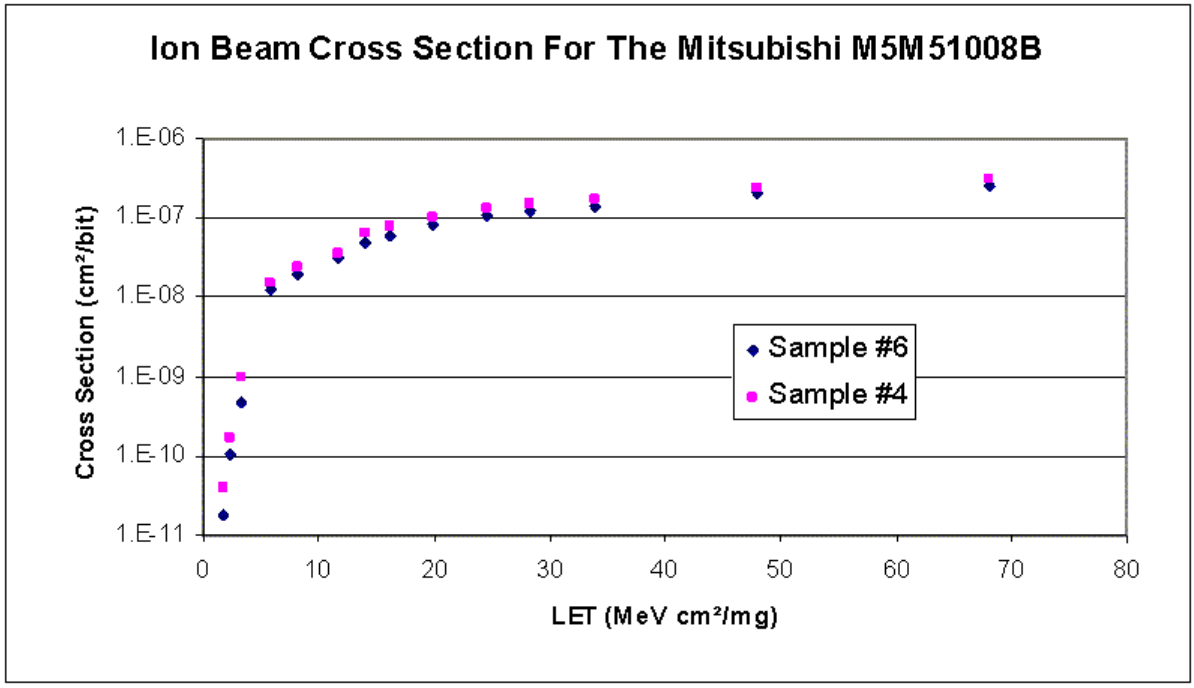

Figure 2.6. Ion beam cross section for the Mitsubishi M5M51008B

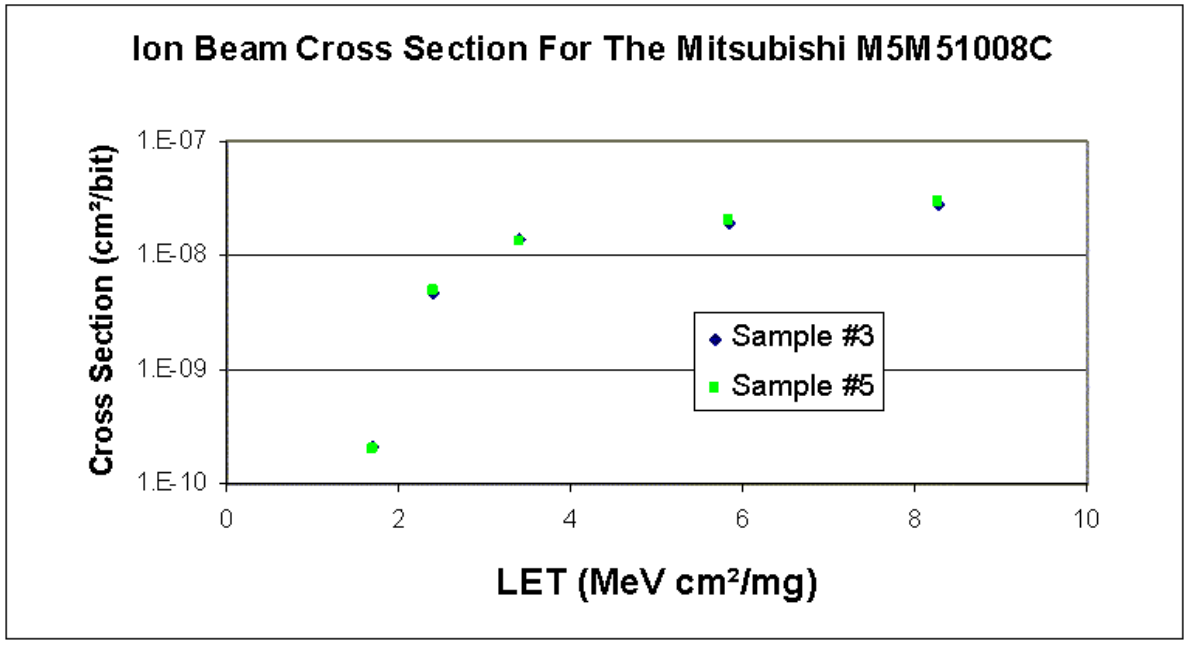

Figure 2.7. Ion beam cross section for the Mitsubishi M5M51008C

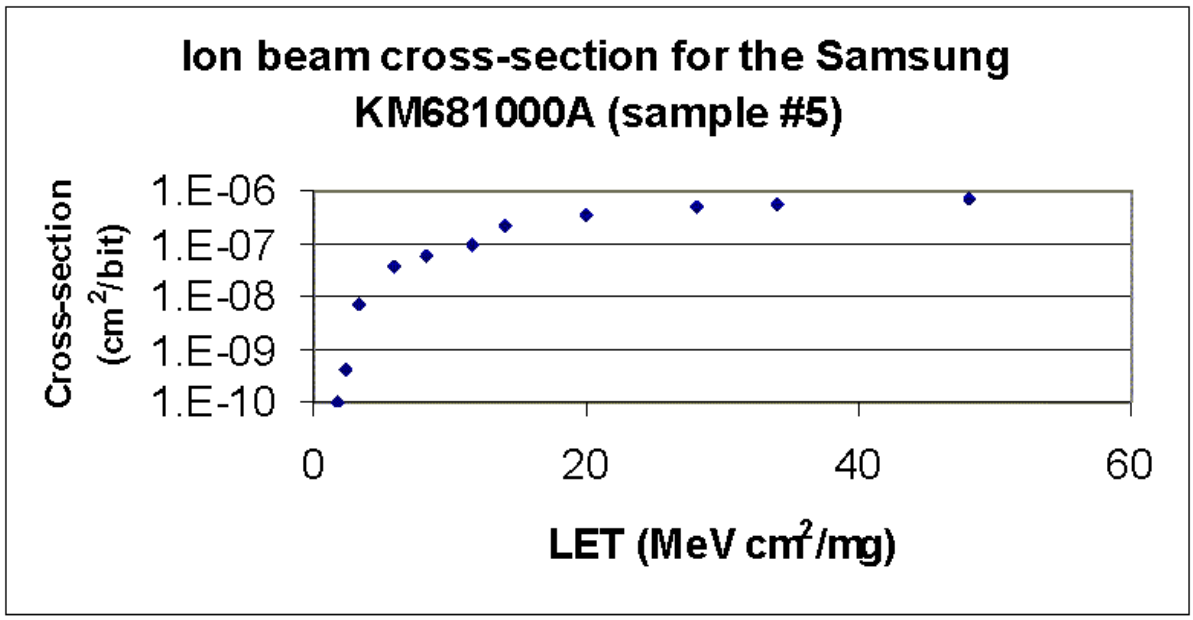

Figure 2.8. Ion beam cross section for the Samsung KM681000A

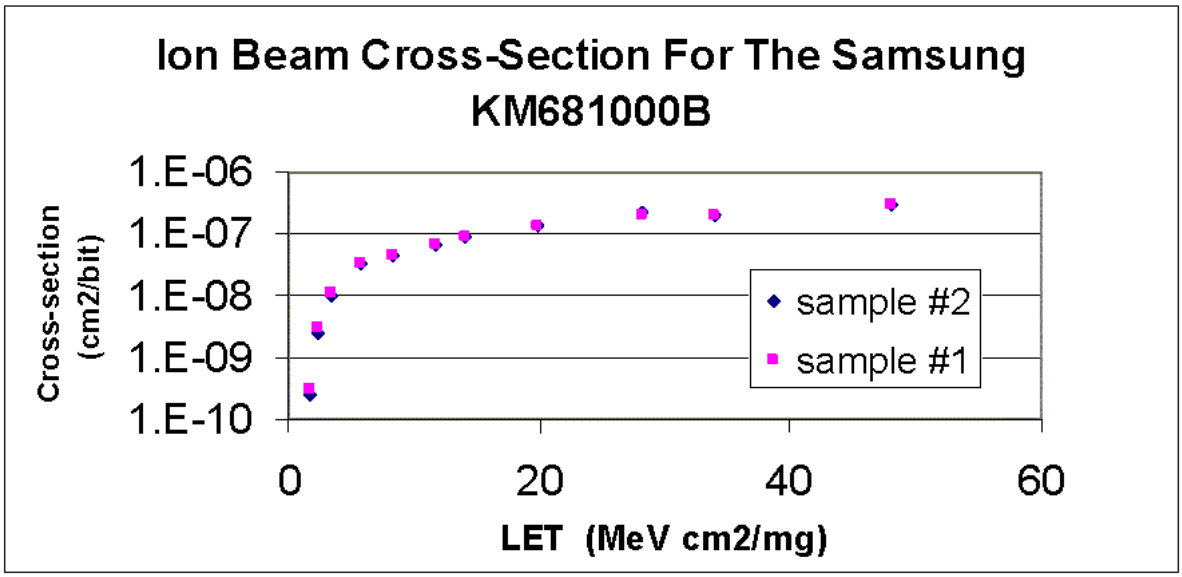

Figure 2.9. Ion beam cross section for the Samsung KM681000B

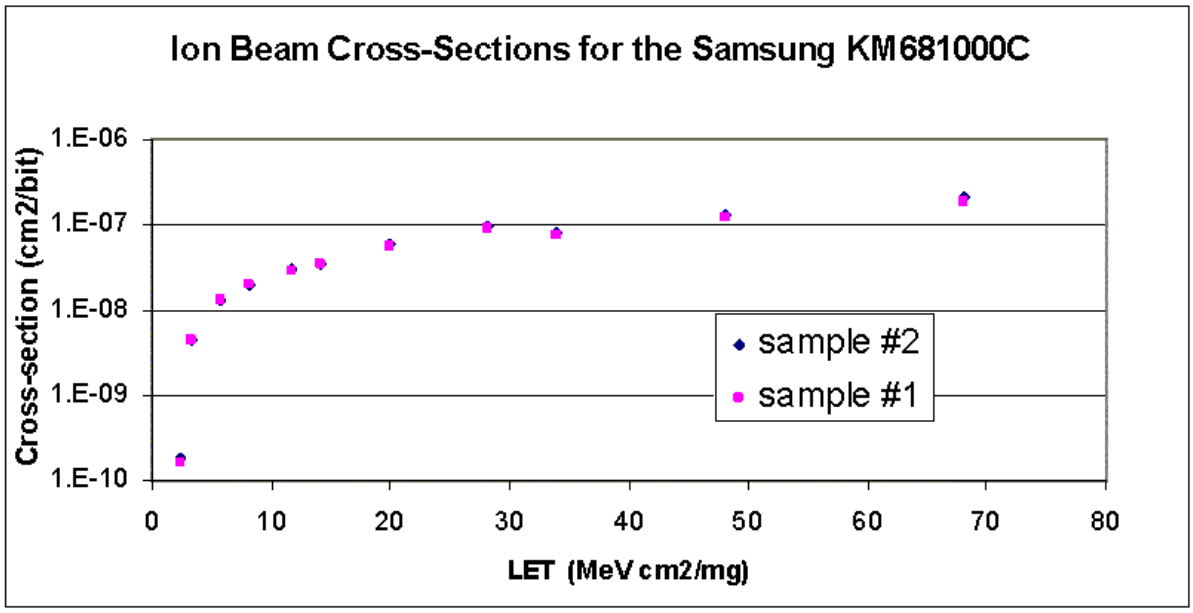

Figure 2.10. Ion beam cross section for the Samsung KM681000C

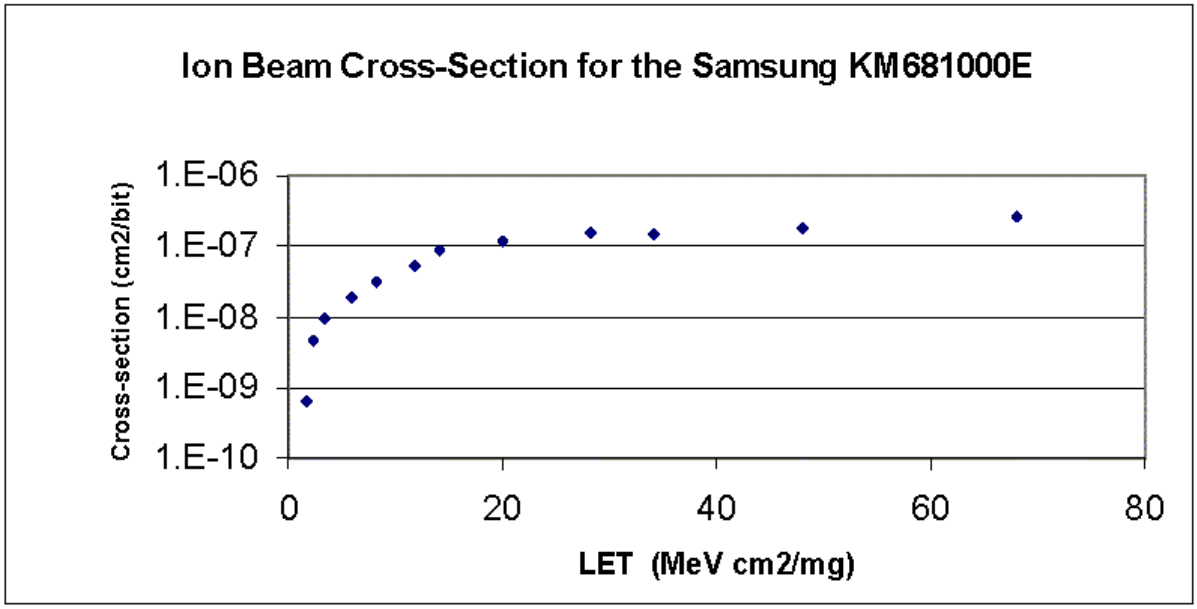

Figure 2.11. Ion beam cross section for the Samsung KM681000E

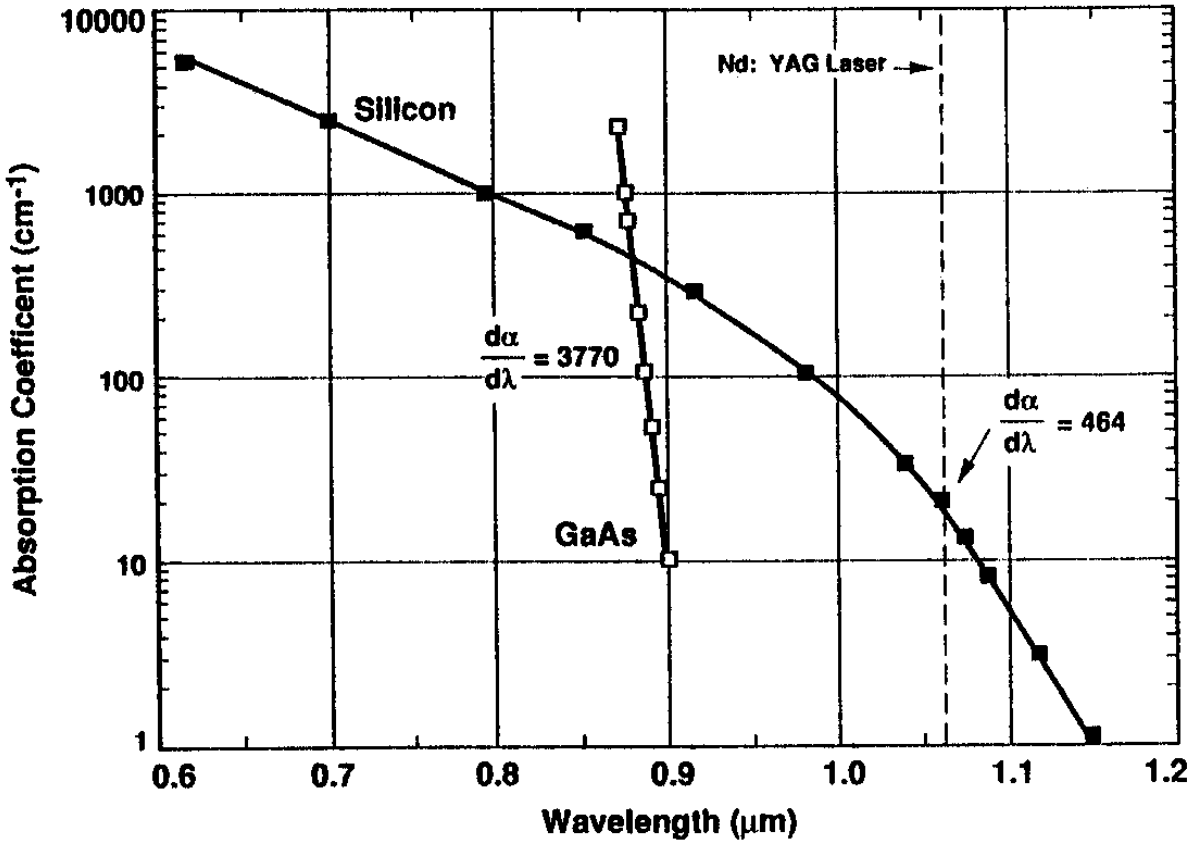

Figure 2.12. The silicon absorptivity as a function of wavelength after A H Johnston, Charge generation and collection in p-n junctions excited with pulsed infrared lasers, IEEE TNS, Vol. 40, No. 6, December 1993.

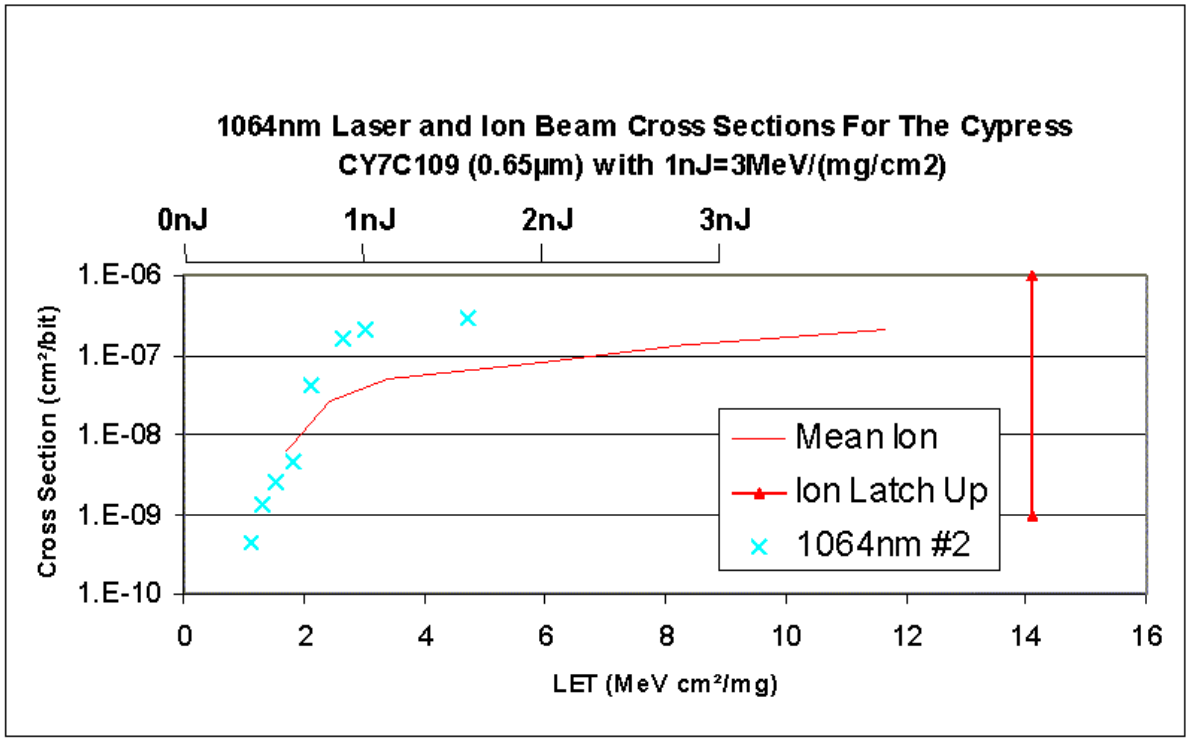

Figure 2.13. Calibration of the infrared results against the ion cross section for the Cypress CY7C109 (0.65µm)

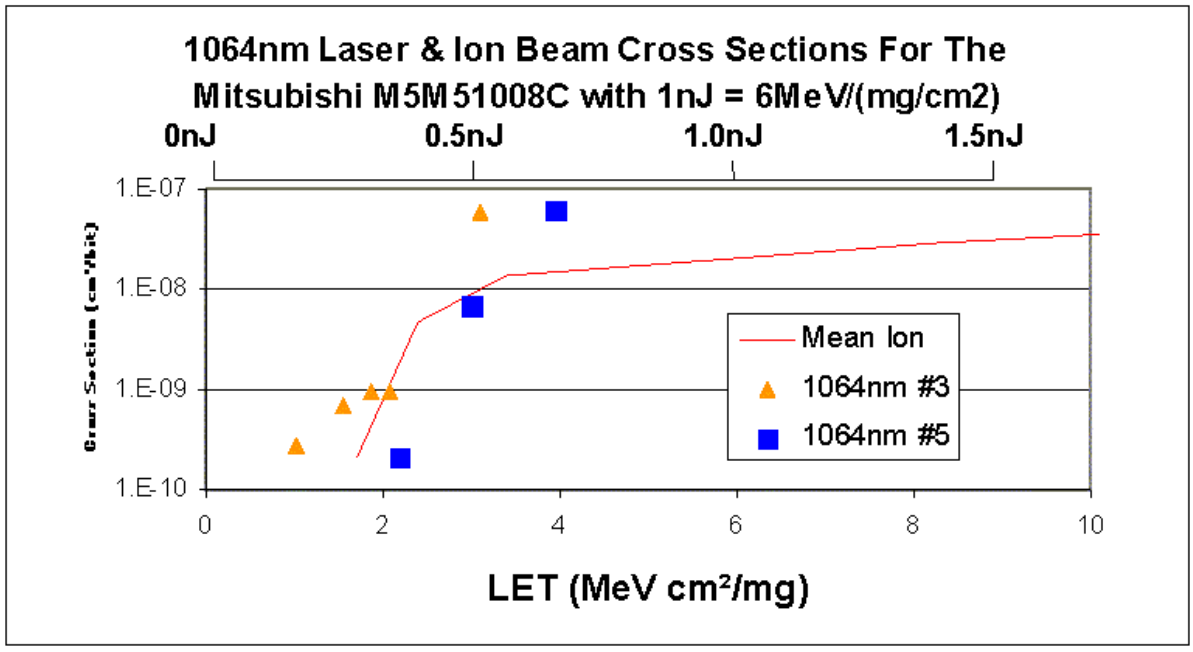

Figure 2.14. Calibration of the infrared results against the ion cross section for the Mitsubishi M5M51008C

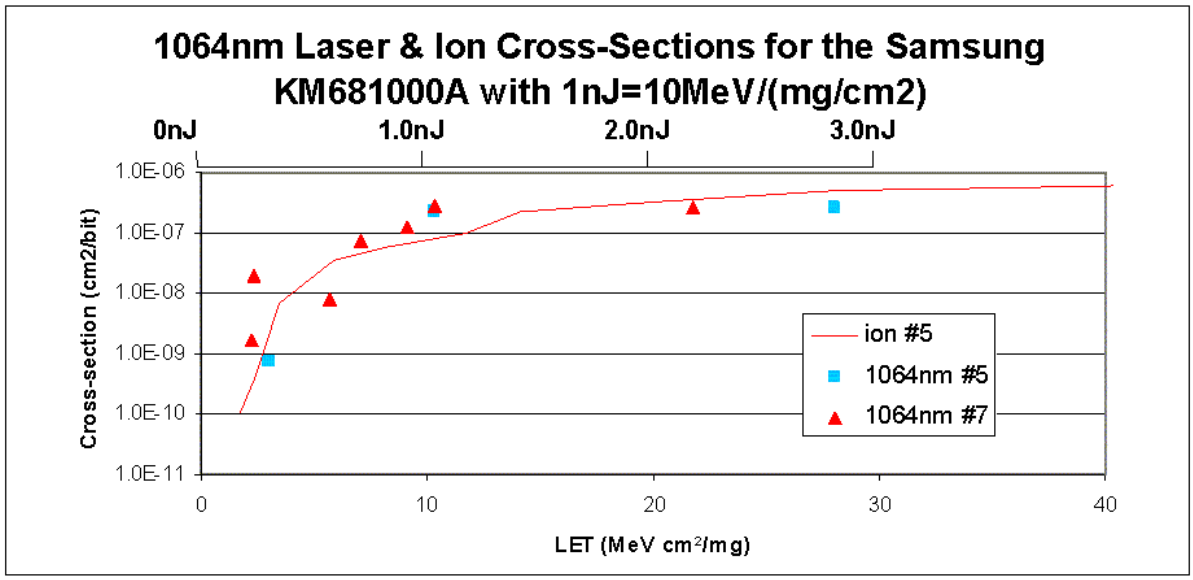

Figure 2.15. Calibration of the infrared results against the ion cross section for the Samsung KM681000A

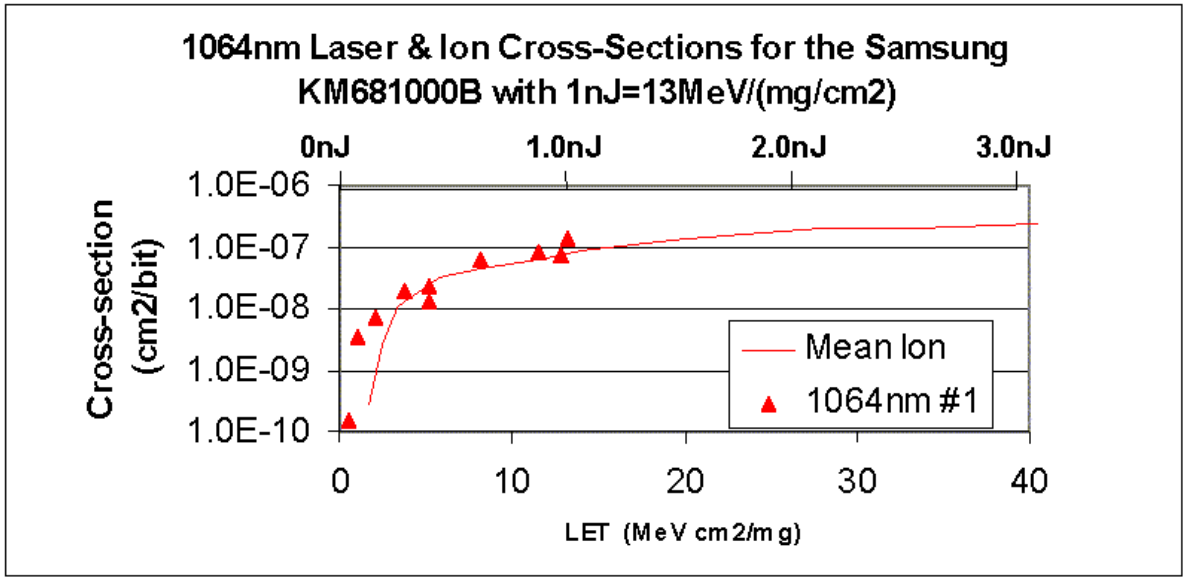

Figure 2.16. Calibration of the infrared results against the ion cross section for the Samsung KM681000B

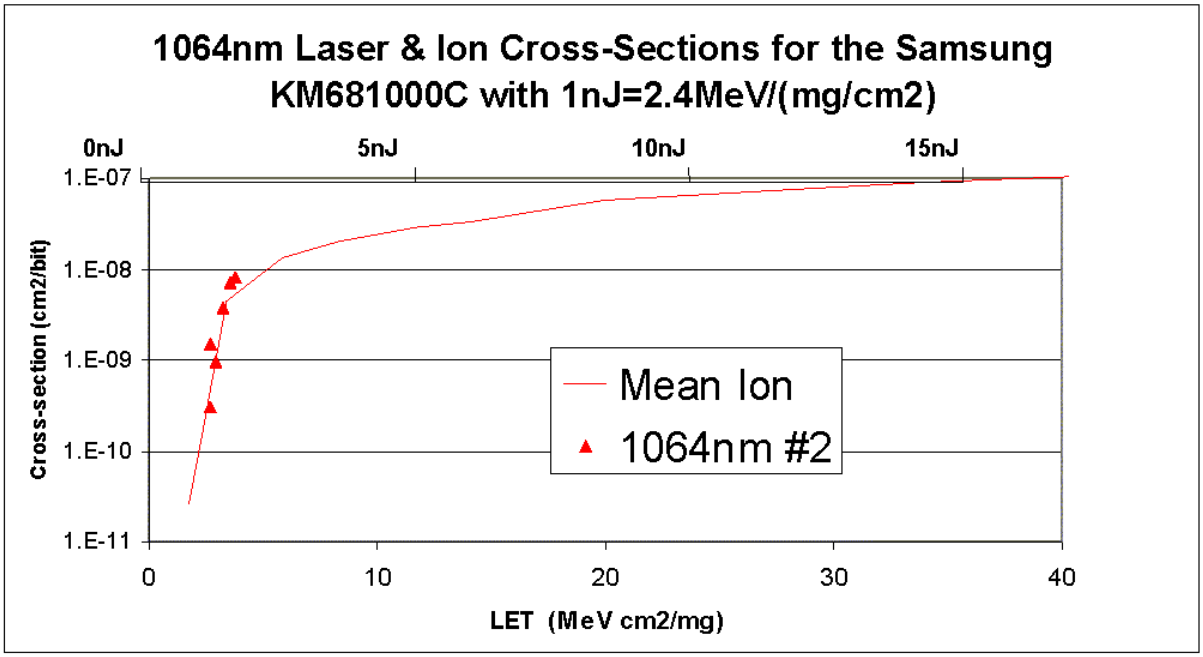

Figure 2.17. Calibration of the infrared results against the ion cross section for the Samsung KM681000C

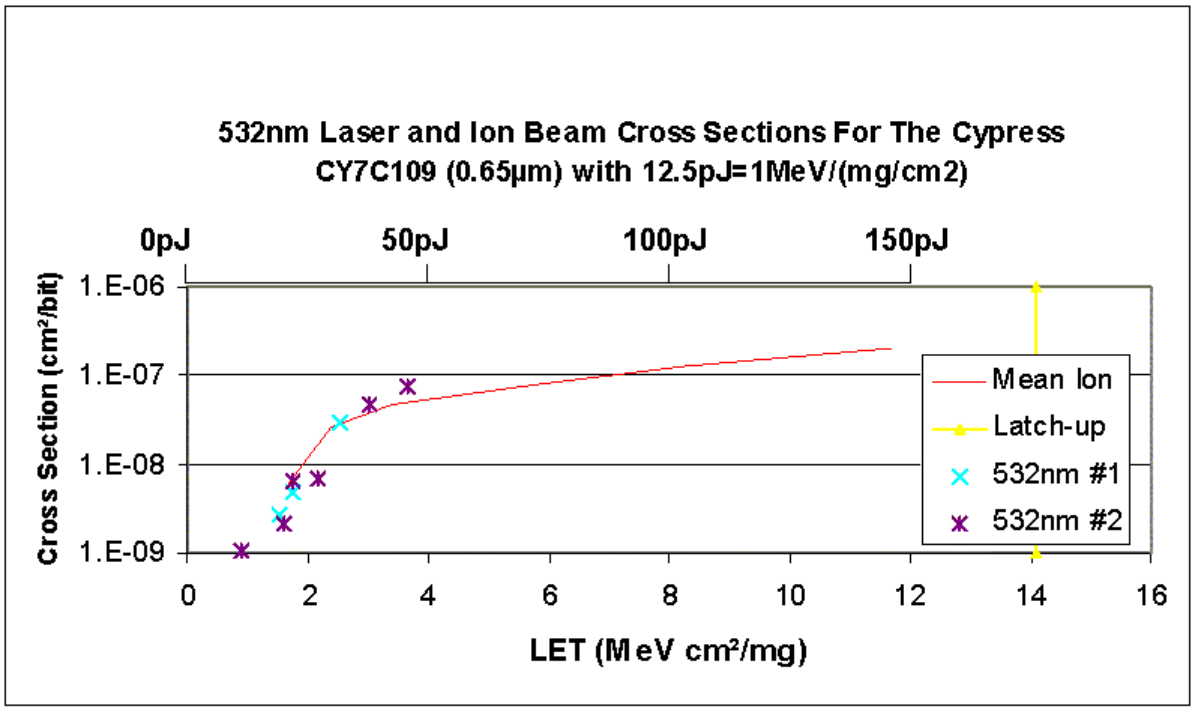

Figure 2.18. Calibration of the green results against the ion cross section for the Cypress CY7C109 (0.65µm)

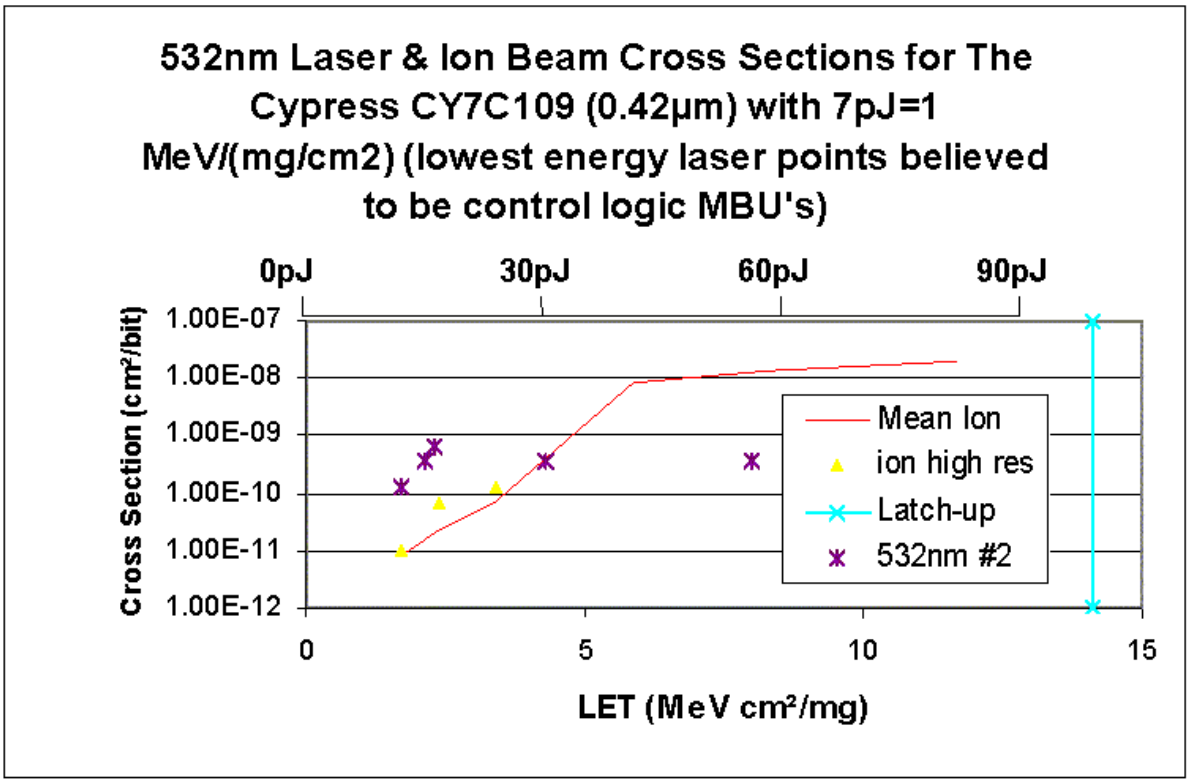

Figure 2.19. Calibration of the green results against the ion cross section for the Cypress CY7C109 (0.42µm)

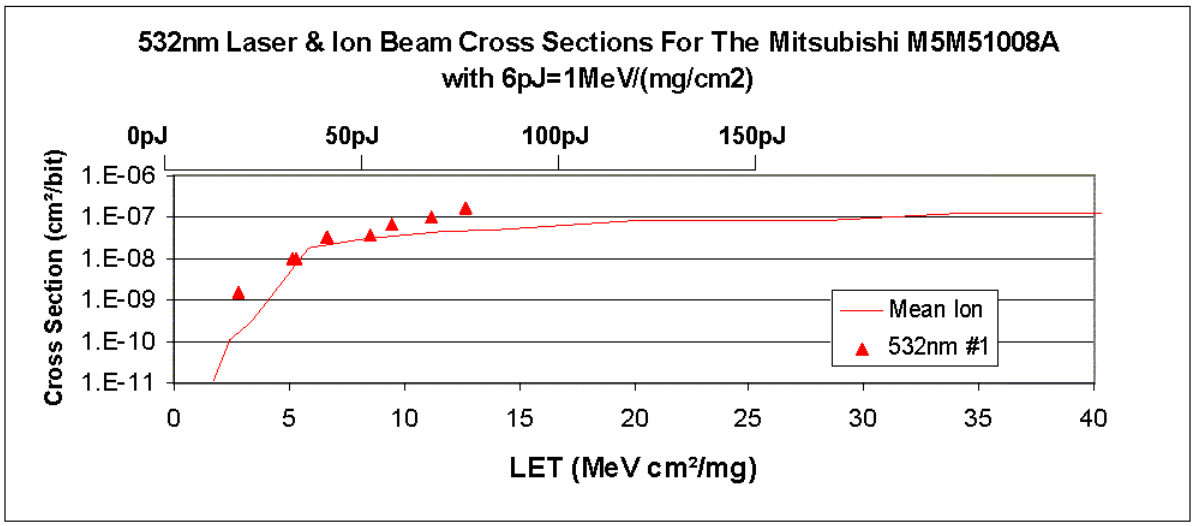

Figure 2.20. Calibration of the green results against the ion cross section for the Mitsubishi M5M51008A

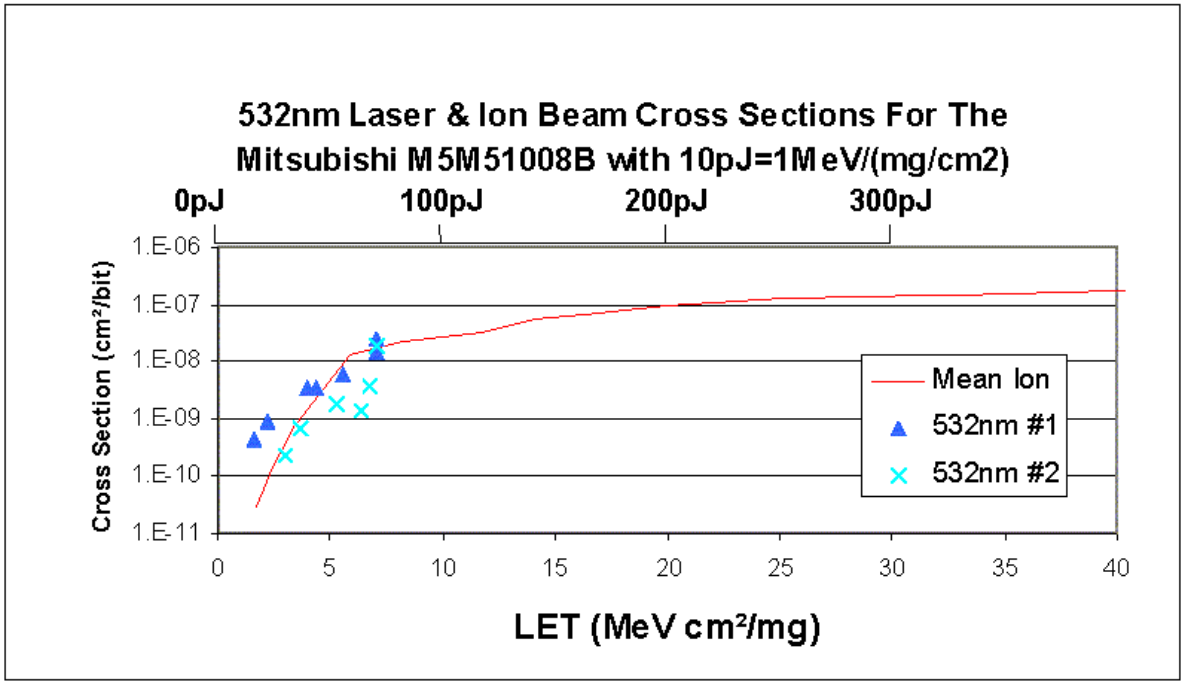

Figure 2.21. Calibration of the green results against the ion cross section for the Mitsubishi M5M51008B

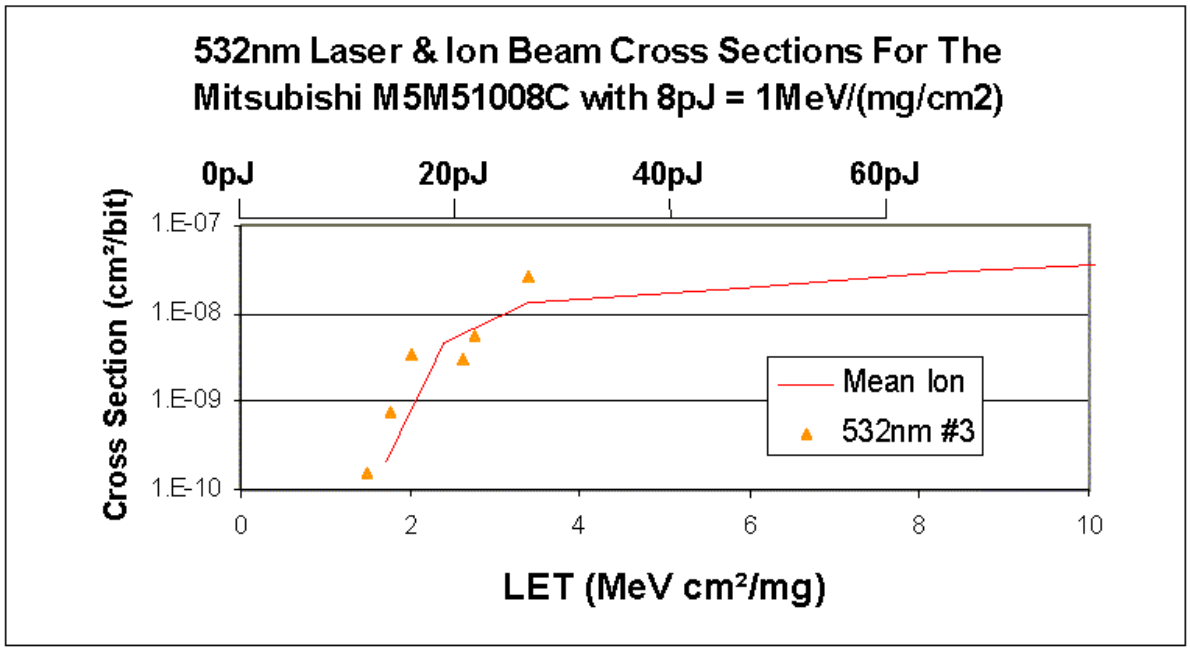

Figure 2.22. Calibration of the green results against the ion cross section for the Mitsubishi M5M51008C

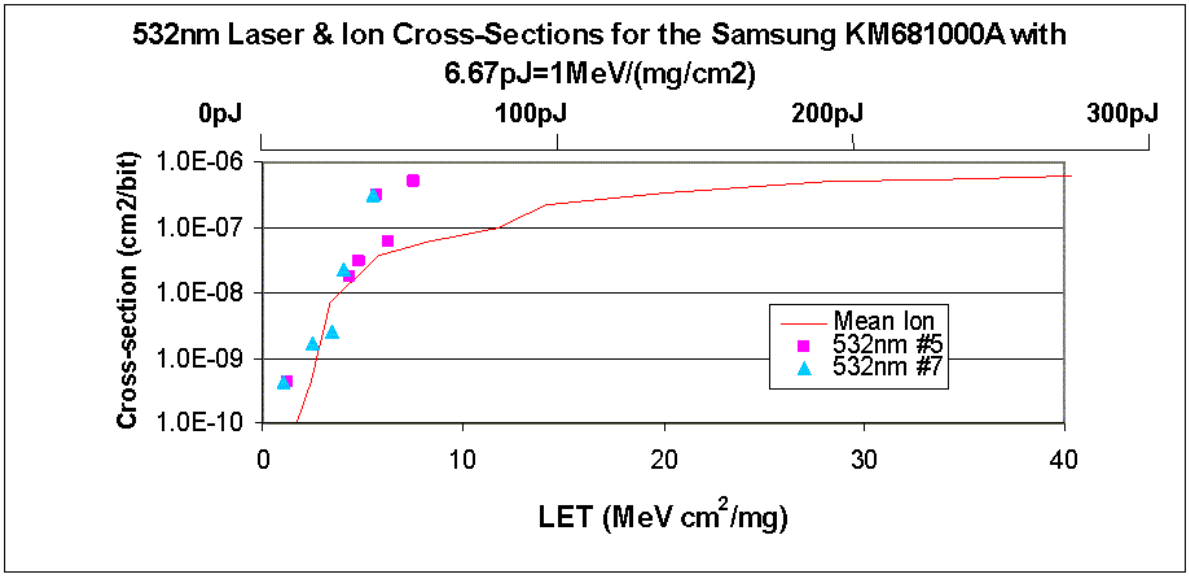

Figure 2.23. Calibration of the green results against the ion cross section for the Samsung KM681000A

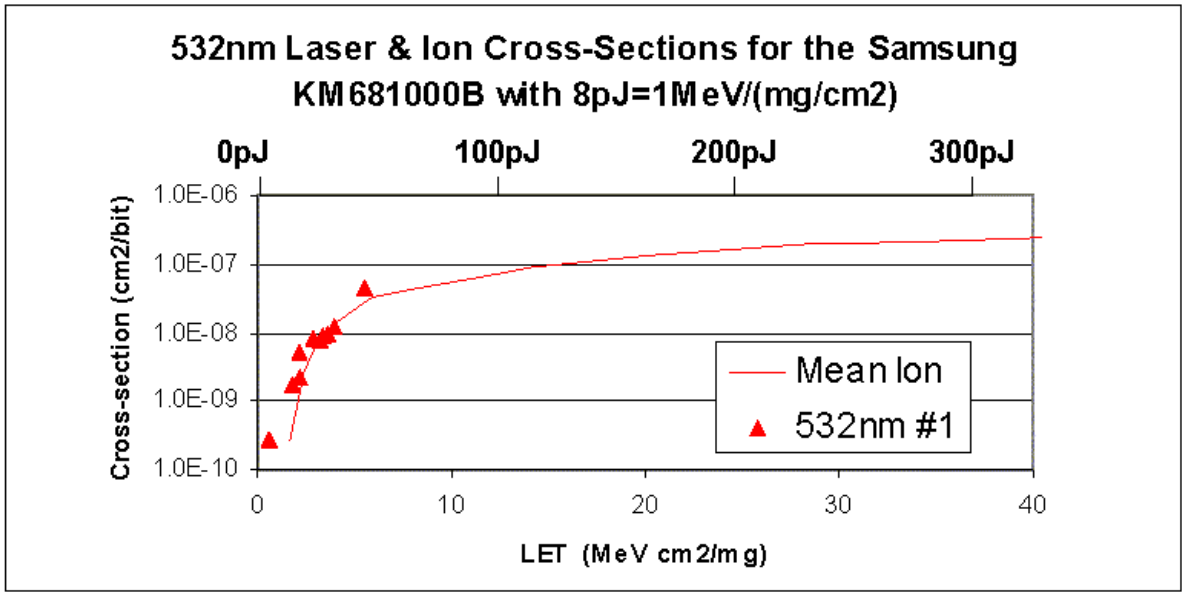

Figure 2.24. Calibration of the green results against the ion cross section for the Samsung KM681000B

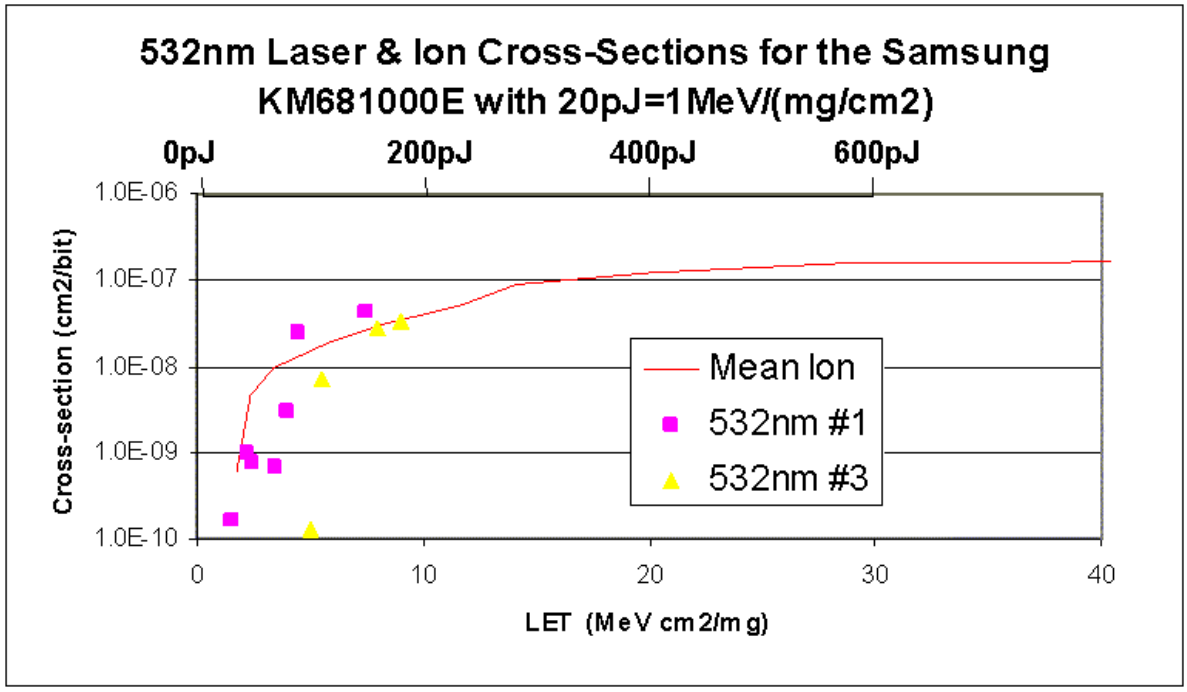

Figure 2.25. Calibration of the green results against the ion cross section for the Samsung KM681000E

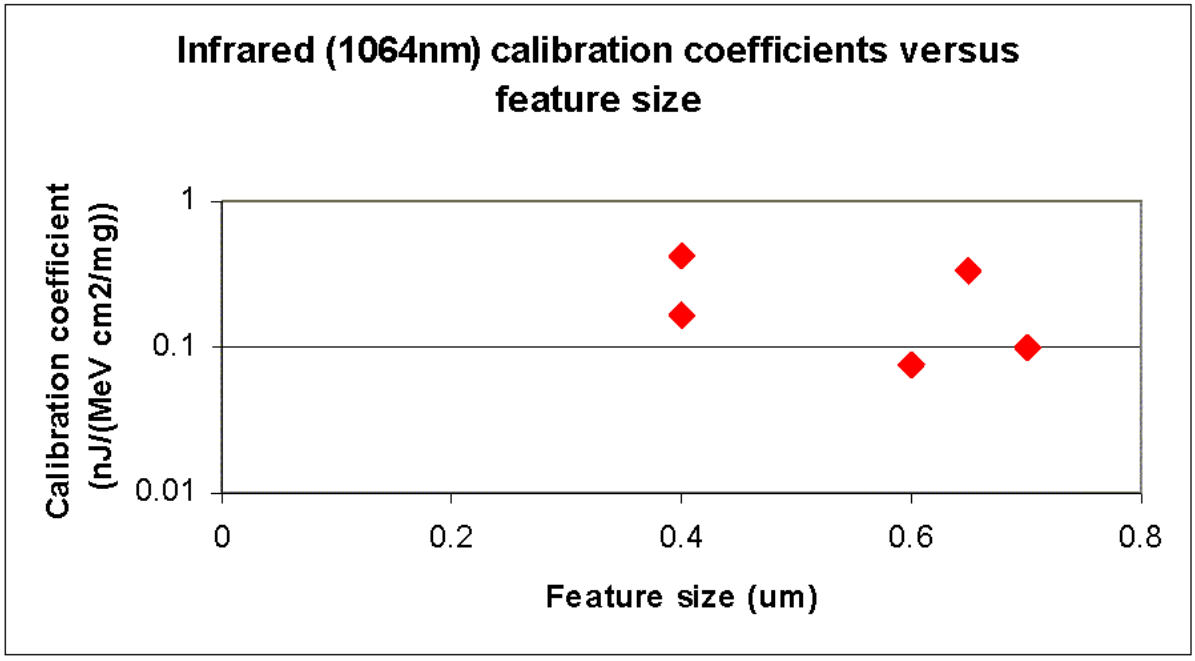

Figure 2.26. Infrared (1064nm) calibration coefficients versus feature sizes for a range of 1Mbit SRAM devices.

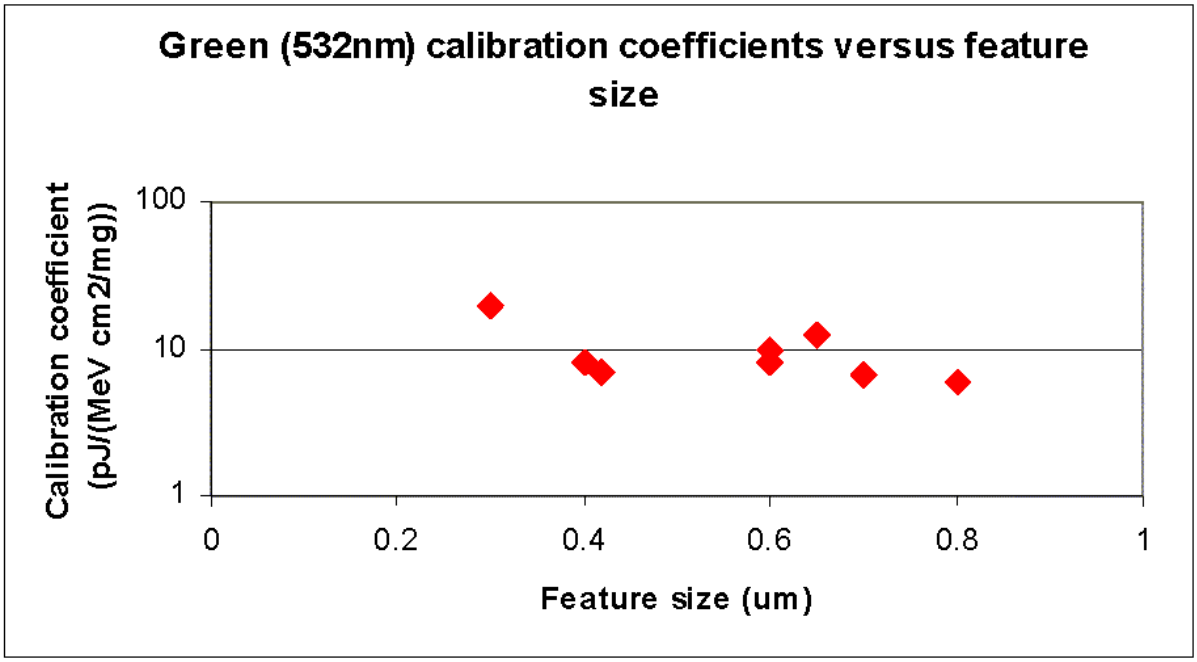

Figure 2.27. Green (532nm) calibration coefficients versus feature sizes for a range of 1Mbit SRAM devices.

3.0 LASER MEASUREMENT OF MICROCHIP SENSITIVITY PROFILES

3.1 Introduction

3.1.1 Laser testing (using large arrays of pulses) can imitate ion beam testing in deriving an LET threshold for upset or latchup (Ref. 3.1). However, the calculation of proton and neutron single event effects further requires a knowledge of the dimensions of the sensitive volume, since the basis of the extrapolation is that proton/neutron effects will be approximately the same as ion effects for the same energy depositions in the sensitive volume. Various approaches have been proposed for combining the sensitive volume information with the LET cross-section curve and proton/neutron interaction physics to derive the proton/neutron upset rate (e.g. Refs. 3.2, 3.3). For instance, C Vial et al have published curves derived using the HETC code (Figure 3.1), which relate the neutron and proton upset rates to the LET upset threshold. However, these curves assume that the proton/neutron strikes a sensitive area and are expressed in terms of the probability per micron of sensitive depth, so a knowledge of the sensitive area and thickness is required to apply them to predict the upset rate in a particular device.

3.1.2 A reasonable estimate of the cross-section of the sensitive volume can be made from the saturation cross-section in ion beam or laser testing provided allowance is made for multiple bit upsets and metallisation shadowing. This leaves a requirement for a measurement of the effective thickness of the sensitive volume. A method of using a beam of carbon ions at a range of energies in order to probe the depth and thickness of the sensitive region has recently been developed and tested by Inguimbert et al (Ref.3.4). The Bragg peak in the ion's energy deposition profile is moved through the sensitive volume by increasing the ion's initial energy. In outline, the location of the sensitive region is inferred from the Bragg peak depth at which the upset rate peaks and its width can be derived from the range of Bragg peak depths over which upsets are observed (Figure 3.2).

3.1.3 The purpose of this section is to show that a measurement of the sensitive depth and thickness can similarly be derived from the laser pulse upset thresholds at a small range of laser wavelengths.

3.2 Theory

3.2.1 The energy deposition profile for laser pulses in silicon is a decaying exponential. At first sight it is not obvious how this type of profile can reproduce the Bragg peak effect to probe the sensitive region depth and thickness. However, on plotting the energy deposition profiles for a range of wavelengths at constant pulse energy, it can be seen (Figure 3.3) that the energy deposition in an arbitrary range of depth (1.3 to 3 microns for the present example) is a maximum at a wavelength in the middle of the range. It transpires that the peak energy deposition wavelength is generally very sensitive to the depth and thickness of the sensitive region.

3.2.2 At a fixed pulse energy, there will in general exist upper and lower bounds on the range of laser wavelengths which give rise to upsets (Figure 3.4). In practice, the most straightforward experimental procedure is to vary the energy at a fixed wavelength to

establish the upset threshold energy for that wavelength.

3.2.3 For pulse energy E_p, reflected energy E_r, sensitive depth D and sensitive thickness Δ, the energy deposited in the sensitive volume is given by:-

$$\int_D^{D+\Delta} \frac{dE}{dx}\, dx = (E_p - E_r)\exp(-f(\lambda)D)(1-\exp(-f(\lambda)\Delta))$$

Where:-

$$\int_0^{\infty} \frac{dE}{dx}\, dx = \frac{1}{f(\lambda)} \left.\frac{dE}{dx}\right|_{\max} = E_p - E_r$$

And $f(\lambda)$ is the silicon absorptivity at wavelength λ.

3.2.4 The energies (E, E') deposited in the sensitive volume at the upset threshold at two (or more) wavelengths (λ, λ') may be equated to form expressions in D and Δ, for example:-

$$E\exp(-f(\lambda)D)(1-\exp(-f(\lambda)\Delta)) = E'\exp(-f(\lambda')D)(1-\exp(-f(\lambda')\Delta))$$

To find unique values of both D and Δ two such expressions are required, which necessitates measurements at three wavelengths.

3.2.5 However, even thresholds obtained for a single pair of wavelengths define a relationship between the sensitive layer depth D and the sensitive thickness Δ. This relationship is plotted for several ratios (5, 15 & 50) of the upset threshold pulse energy in infra red (1064nm) to that in green (532nm) in Figure 3.5. Note that a ratio of 50 would imply that D<2.3µm and Δ<10µm.

3.3 Generalisation of the Technique

3.3.1 The sensitive volume concept that a rectangular region of uniform sensitivity may be associated with each cell of the device is, of course, a gross simplification. In reality the cells are somewhat amorphous regions of continuously varying sensitivity and it is quite possible that there may exist two or more peaks of sensitivity within these regions. However, it can be shown that the laser technique actually incorporates the potential explicitly to measure the precise depthwise variation in the sensitivity of cells.

3.3.2 If the sensitivity is defined as an unknown function sens(x) of the depth x beneath the silicon surface of the device, then the critical charge deposition Q_{crit} for upset to occur may be expressed as an integration over the product of sens(x) with the upset threshold laser pulse energy deposition rate at depth x. This laser energy deposition rate dE/dx is proportional to the absorbed laser pulse energy at the upset threshold E_{abs}, which may be expressed as a function of the silicon absorptivity $E_{abs}(f(\lambda))$, since it will be different for each test wavelength. We may write:-

$$\frac{dE}{dx} = E_{abs}(f(l))f(l)\exp(-f(l)x)$$

Hence,

$$Q_{crit} = \int_0^\infty E_{abs}(f(l))f(l)sens(x)\exp(-f(l)x)dx$$

On rearranging:-

$$\frac{Q_{crit}}{E_{abs}(f(l))f(l)} = \int_0^\infty sens(x)\exp(-f(l)x)dx$$

3.3.3 The critical charge for upset may be assumed to be constant at all wavelengths (this may not quite be strictly true in all circumstances, but it is usually a good approximation) and the absorptivity is a well-known function of wavelength. Thus the left-hand side of the equation may be calculated empirically simply by measuring the absorbed laser pulse energy at the upset threshold for a wide range of wavelengths (i.e. for a wide range of absorptivities). Now the right-hand side of the equation is just the Laplace transform of the depthwise sensitivity profile in the absorptivity, hence sens(x) may in principle be derived by performing an inverse Laplace transform on the left-hand side result.

3.3.4 It should finally be noted that the reciprocal of the absorptivity 1/f(λ) provides a scale length for the distance over which the laser light is absorbed in the silicon. To obtain good results from this technique it will be necessary to test devices using laser pulses over a wavelength range such that 1/f(λ) varies from being smaller than the size of the smallest sensitivity features that are to be resolved to being larger than the overall size of the sensitive region.

3.4 Advantages of the Laser Technique

3.4.1 In the ion beam approach to the measurement of the sensitive volume thickness, there is a risk of ions of the chosen species still causing upsets at near saturation levels after the Bragg peak has penetrated beyond the sensitive region. This would make it very difficult to get an accurate thickness as well as a depth for the sensitive region. Essentially it is necessary to choose an ion species with an LET in the Bragg peak which is just fractionally above the upset threshold for the device in order to obtain accurate results. This problem does not arise with laser pulses, because the pulse energy is trivially, continuously and precisely variable, such that pulse energy at the threshold may be measured at each experimental wavelength. Furthermore, the silicon absorptivity is such a strong function of wavelength that there is no real difficulty in varying the penetration of the laser pulses over the requisite range.

3.4.2 A further potential advantage of the laser technique is that it excludes metallisation

layers and passivation oxide from the depth measurement. The laser spot is focussed on the silicon surface and will only penetrate where there is silicon. Ions may experience more variation in the effective depth of the sensitive volume across the chip surface, which could lead to additional experimental error. In general, the increased flexibility and precision of the laser technique combined with the lower capital cost of the laser equipment would be expected to make it preferable to the ion beam methodology in most circumstances.

3.5 Analysis of Measurements

3.5.1 The ratios of the pulse energy thresholds in green and infrared given in Table 2.2 are susceptible to a degree of analysis on the basis of this theory. The threshold pulse energies for infrared upset were between a factor 9.62 and 26.67 greater than the corresponding pulse energy thresholds for green laser light. Referring to Figure 3.5, it may be noted that the curve for a ratio of 15 is not far from these results.

3.5.2 In parallel, NMRC has performed detailed constructional analyses on samples of the same devices (from the same batches) (Ref. 3.5). The cross-sectional view of the M5M51008CFP shown in Figure 3.6 is an example of this work. The component is fabricated using a 0.35μm p-well process utilising two levels of metallisation and four levels of polysilicon on a non-epitaxial substrate, producing TFT-load SRAM cells. It was established that the n-channel transistor diffusion depth was 0.1μm and the well was 1.8μm deep. This sensitive region lies immediately beneath the gaps in polysilicon layer number 1 in Figure 3.6. However, in this design the cell loads are composed of p-channel thin film transistors formed from the overlying poly 3 and poly 4 layers. Furthermore, funnelling may enable charge to be gathered even from the substrate beneath the well and the materials in which the polysilicon layers are embedded are observed to be optically transparent. Consequently, the real picture is one of a varying profile of sensitivity over a depth range larger (perhaps much larger) than 2μm, possibly with two (or more) peaks for the different transistor elements in the cell. Clearly, there is no precise correspondence between observable features and the boundaries of the sensitive volume. For example, there seems to be no correlation between the pulse energy ratios and the NMRC well depth values or the feature sizes (Table 3.1).

3.5.3 The NMRC results for all the devices suggest that the effective sensitive depth should really be quite small, i.e. probably a micron or less. This is because the depletion layers and the associated wells all start from the base of the transparent material. With reference to Figure 3.5, it may be seen that a small sensitive depth implies a relatively large sensitive thickness. In particular, ratios near 15 are only consistent with a sensitive thickness of 10μm or more if the sensitive depths are small. Furthermore, this result is not very susceptible to error, since the ratios would need to be an order of magnitude larger for the sensitive thicknesses to be consistent with the well depth. The conclusion must be that charge is probably being gathered into the cells from deep into the substrate via the funnel effect (see Figure 3.7). It should be noted that this conclusion is consistent with the independent observation based on the green calibration factors that the sensitive thickness is not scaling with feature size. This may be an important observation for the future of SEE testing and hardening.

3.6 Metallisation Interference and Measurement of Reflectance

3.6.1 It should of course also be mentioned that the usual laser problems of metallisation potentially shadowing some sensitive areas or reducing the energy reaching sensitive regions continue to apply. One approach to correcting for metallisation may be to calculate or measure reflections of laser pulse light from the chip surface. Some such measurement is anyway necessary, due to the complex reflections from the oxide and silicon surfaces. An accurate means of determining the proportion of reflected pulse energy is clearly essential for accurate results. This issue has been discussed in Section 2.6.

3.6.2 Account may sometimes need to be taken of the influence of doping concentrations on silicon absorptivity at the longer infra red wavelengths, but there is no evidence for significantly increased absorptivity in the present results. This would give relatively lower laser pulse energy upset thresholds and the thresholds are actually a little higher than the theoretical equivalent laser LET would suggest.

3.6.3 There has been a view that increasing numbers of layers of metallisation will soon obscure the die surface to such an extent that laser pulsing through the front surface will become impossible and pulsing will have to be performed through the (polished) back surface of the microchip die. However, the results presented here do not completely support this view. The NMRC analyses show that metallisation is conventionally arranged in layers of tracks with gaps between the tracks in each layer and gaps between the layers. This means there will always normally be a path through the gaps to the silicon, even for large numbers of layers, but the path will normally be tortuous and indirect rather than line of sight. Nevertheless, light and light delivered energy does not necessarily travel in straight lines on the micron scale of its wavelength. In fact diffraction, charge diffusion and internal reflections in the metallisation array are probably collectively quite effective at transmitting energy through the gap paths, so the simplistic "geometrical optics" view that a line of sight path is necessary for laser energy to reach the silicon may not be true. Actually, there is little evidence in the present results of any difficulty in inducing upsets. All the devices except the FPGA were easily upset. In the case of the FPGA (see Section 4) the problem is unlikely to be due to metallisation obscuration, especially because ion induced upsets were not seen in this device either. It may tentatively be concluded that metallisation obscuration is a less severe constraint than had been believed, but that very sophisticated reflected light monitoring may be necessary to maintain energy calibration in the future.

Part No	Manufacturer & Feature Size	Threshold energy ratio 1064:532nm	Well thickness (µm)
CY7C109	Cypress 0.65µm	26.67	5.4
M5M51008C	Mitsubishi 0.4µm	20.83	1.8
KM681000A	Samsung 0.7µm	14.99	6
KM681000B	Samsung 0.6µm	9.62	3.8

Table 3.1. Summary of SRAM pulse energy ratios with NMRC well thicknesses.

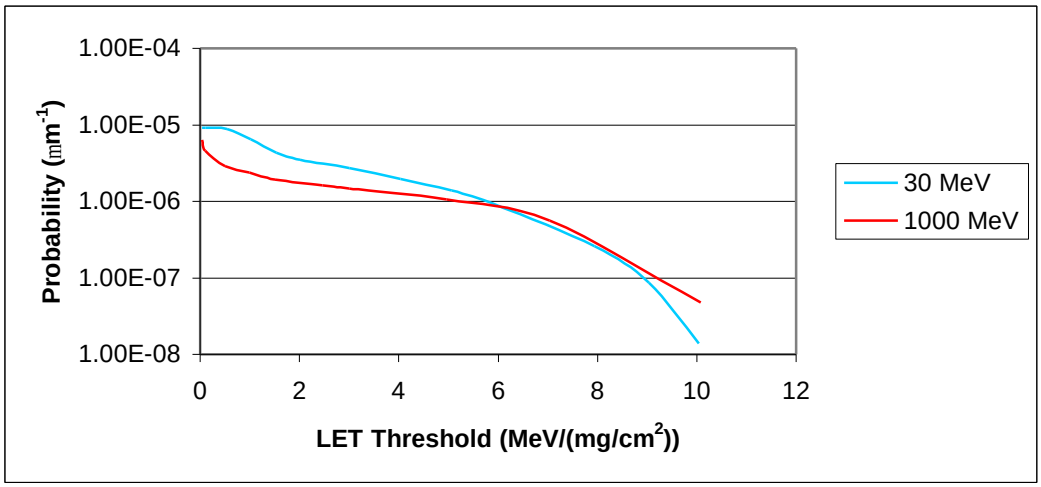

Figure 3.1. Neutron upset probability as a function of LET threshold for ion induced SEU.

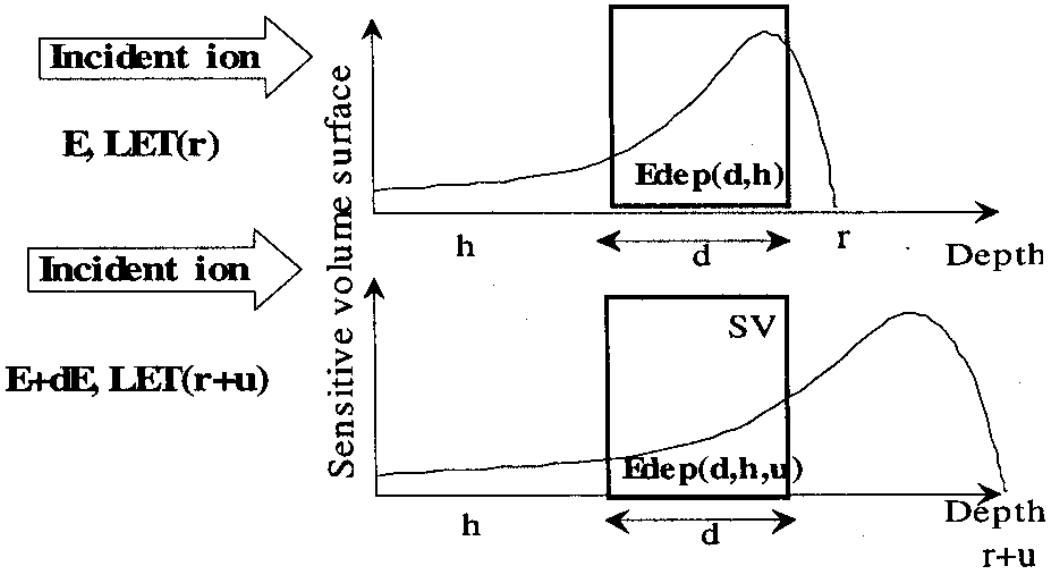

Figure 3.2. Carbon ion beam probing of the sensitive volume.

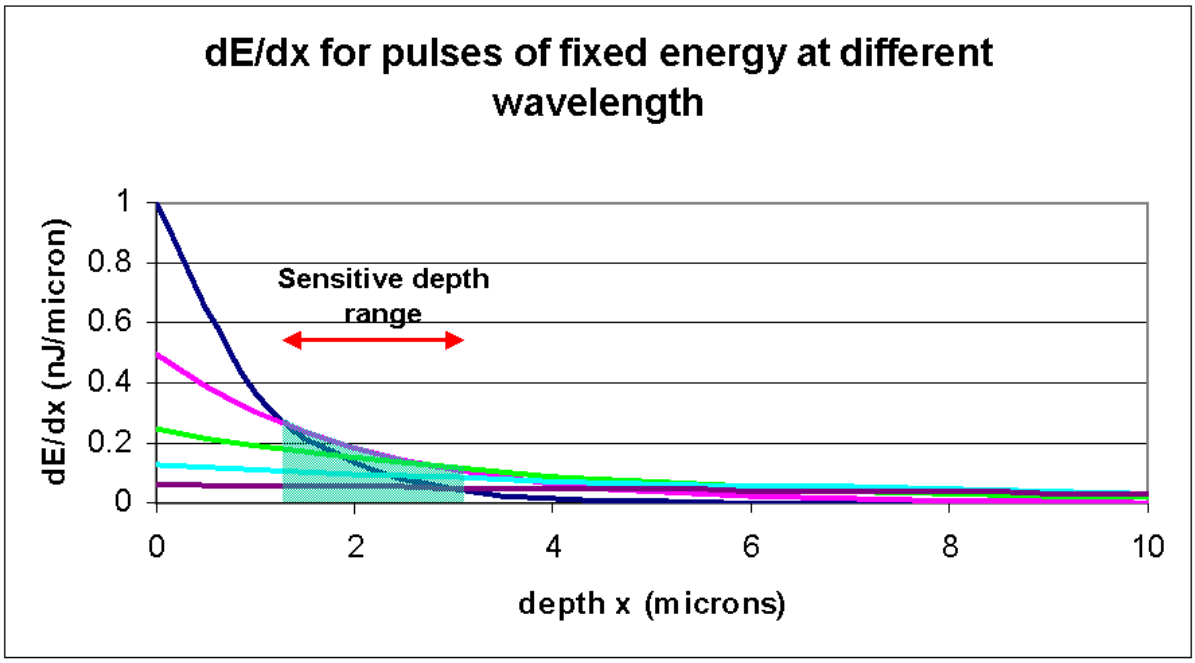

Figure 3.3. dE/dx for laser pulses of fixed energy at a range of wavelengths (green to infra red)

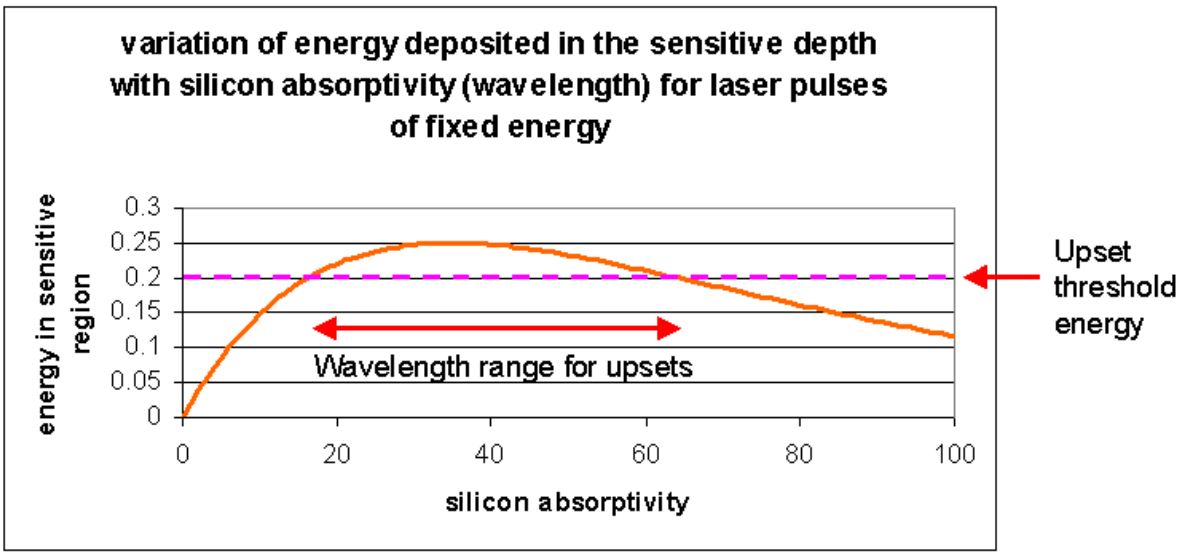

Figure 3.4. Variation of energy deposited in the sensitive layer with silicon absorptivity for laser pulses at a fixed energy (conceptual)

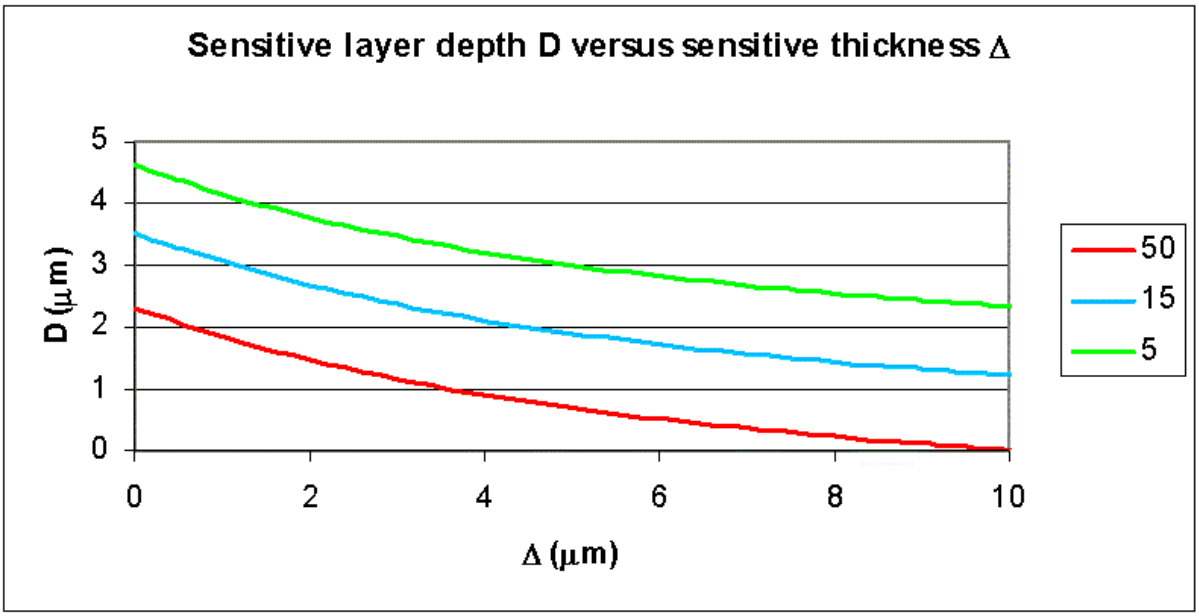

Figure 3.5. Sensitive layer depth D versus sensitive layer thickness Δ at three upset threshold ratios (1064nm:532nm)

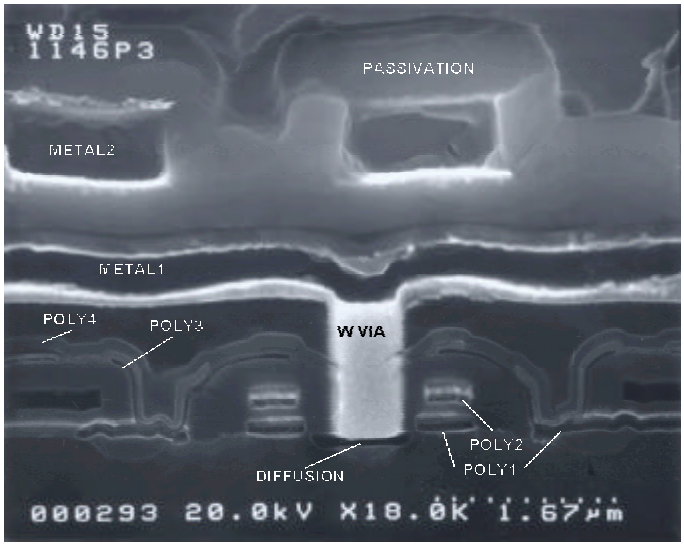

Figure 3.6. Cross-sectional view of the M5M51008CFP (x18000: the dotted scale is 1.67µm)

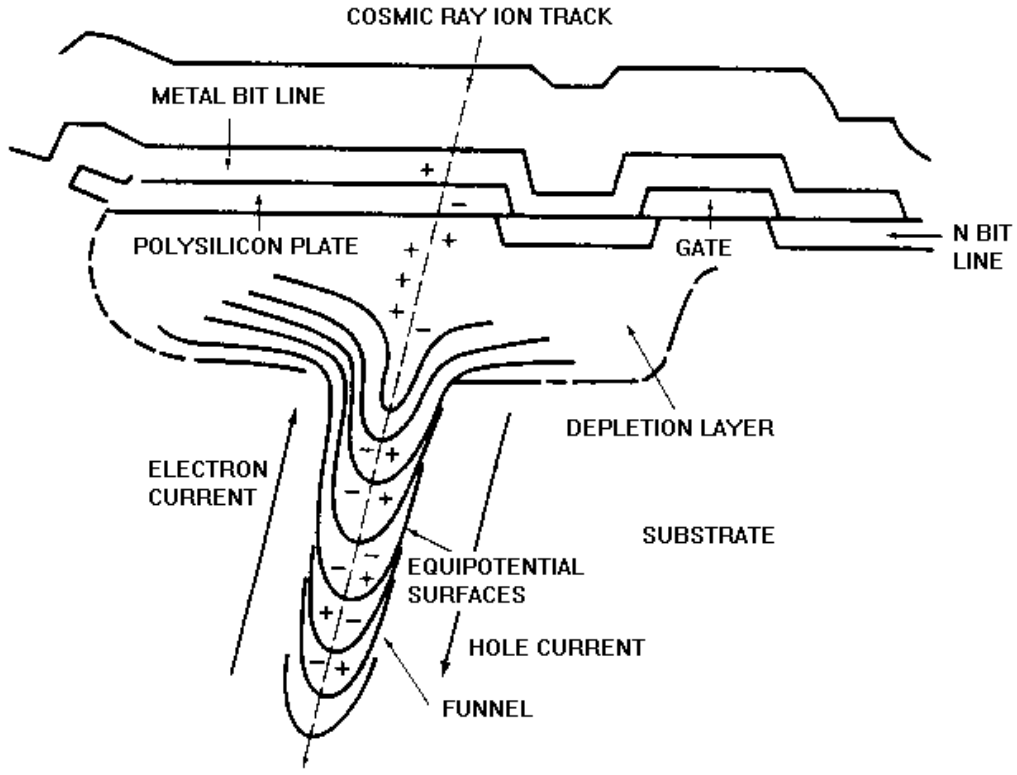

Figure 3.7. Gathering charge from the substrate via the funnel effect.

4.0 LASER TESTING OF AN FPGA

4.1 Introduction

4.1.1 At the RADECS 99 conference Lloyd Massengill gave an invited talk on Opportunities for Single Event Modelling in Emerging Commercial Technologies. He placed considerable emphasis on efforts to model single event effects in combinatorial logic devices (FPGA's, ASIC's etc.), which pose a special testing problem, since the ultimate error event may arise at a greatly different location in the device than the single event stimulus. Laser testing provides a possible validation methodology for this kind of modelling. Alternatively, laser testing may offer a special advantage over other types of testing for these devices, because of its special property of allowing the physical location of the SEE stimulus to be chosen precisely.

4.1.2 The Radiation Effects Group has therefore selected an FPGA device, designed a test circuit for the device and blown two samples with this circuit (a third sample was retained as a control). The device was then submitted to SEREEL laser testing to investigate the viability of the laser as a testing tool for combinatorial logic.

4.2 Device Selection and Test Circuit Design

4.2.1 Various ASIC's and FPGA's were considered for use in this study. However, the ACTEL 54SX16 FPGA was selected by virtue of the combination of recent experience of this device by the Group and the willingness of ACTEL to support the investigation by blowing a test circuit and by providing of an outline die map of the test circuit.

4.2.2 A simple test circuit was designed as defined by the circuit diagram of Figure 4.1. A sixteen line data bus was generated, where the first four lines were derived from a register with the data being clocked in from external inputs (Figure 4.2). The remaining lines were generated by a set of three 4-bit counters (Figure 4.3), which were incremented by an external clock. The stream of 16-bit data words thus generated were decoded into four outputs by a set of four logic decoders, which were implemented with small networks of AND and OR gates (Figures 4.4 to 4.7). Finally, two special networks of AND and OR gates were employed to detect certain kinds of gross upsets where all the lines went high or low simultaneously (Figure 4.8).

4.2.3 The objectives of this circuit design were several. Firstly, components which store data (the counters and the register) were necessary, since storage elements effectively latch transient upsets into the circuit's "memory", hence making the consequences of upsets pseudo-permanent and readily observable. Secondly, gate networks, which transmit and modify errors, were required in order to simulate the equivalent behaviours in real systems. For example, these arrays have been designed to include similar amounts of AND and OR logic, because AND logic tends to suppress errors whereas OR logic tends to exacerbate their consequences. In general a given counter or register error induced by a laser pulse may or may not upset an output with a probability which depends on the details of the logic networks as well as on the intrinsic susceptibility of the counter or register. Finally, the circuit has been designed to have many possible states with differing intrinsic susceptibilities to SEE to mimic

this additional dimension of complexity found in real applications of these devices.

4.2.4 The circuit was blown in three samples by Actel (Joe Wells), who also furnished a map of the location of the circuit elements on the microchip die. The plan was to generate SEE's by targeting specific circuit elements with the laser. The device was clocked with the chosen data input prior to testing, so as to generate the correct output data stream. Thus output errors were readily diagnosable when the output data stream during testing differed from this pre-recorded stream.

4.2.5 Testing was initially performed at the UCL ion beam facility, but this failed to produce any error events. However, the LET's and the ion fluences for these tests are reproduced in Table 4.1.

4.3 Laser Testing

4.3.1 Laser testing was conducted with 40ps focussed pulses at both the infrared (1064nm) and green (532nm) wavelengths. However, despite very extensive testing up to very high laser pulse energies, no errors were observed in the vicinities of the counters or the register or anywhere else among the main FPGA elements. The maximum pulse energy in infrared testing reached 3.4μJ, at which level one of the samples was destroyed, but no errors were seen prior to its destruction. The green laser testing ranged up to several nJ without observing any errors among the main FPGA elements.

4.3.2 In order to try to sensitise the device to SEE, the supply voltage was reduced by raising the ground level. This did indeed generate sporadic errors, but they were found to occur whether or not the laser pulses were being delivered.

4.3.3 Laser testing was also repeated on the Group's dose rate laser system, which delivers nanosecond laser pulses at 1064nm across the whole device die. No errors were seen in this testing either up to a dose rate equivalent of 8E9 Rad(Si)/s. This tends to confirm that the Actel 54SX16 is indeed very resistant to transient radiation effects.

4.3.4 Several SEE sensitive areas were ultimately identified whilst testing a strip at one edge of the device using green pulses at an energy of 2.4nJ. These results have been summarised in an image of part of the device annotated with the sensitive sites and an indication of the errors which were observed (Figure 4.10). A mismatch in the output data stream as against the pre-recorded stream was recorded as an error. The usual type of error was a jumping of the output sequence N cycles forward of the expected position, where N was an integer, which varied from case to case and was sometimes negative (i.e. jumped back N cycles). These mismatches persisted in the subsequent data streams until a reset signal was sent to the device, except that depowering was required to clear the error in case number 5 and the device suffered a lock-up event (possibly a latchup) in case number 3.

LET (MeV/(mg/cm^2))	Fluence (ions/ cm^2)	Irradiation time (s)
14.0	251000	118
16.2	256000	122
19.8	1000000	432
21.8	1000000	309
34.0	1000000	195
34.0	5000000	520
52.9	5000000	871

Table 4.1. Ion beam testing of the Actel 54SX16 FPGA (no errors).

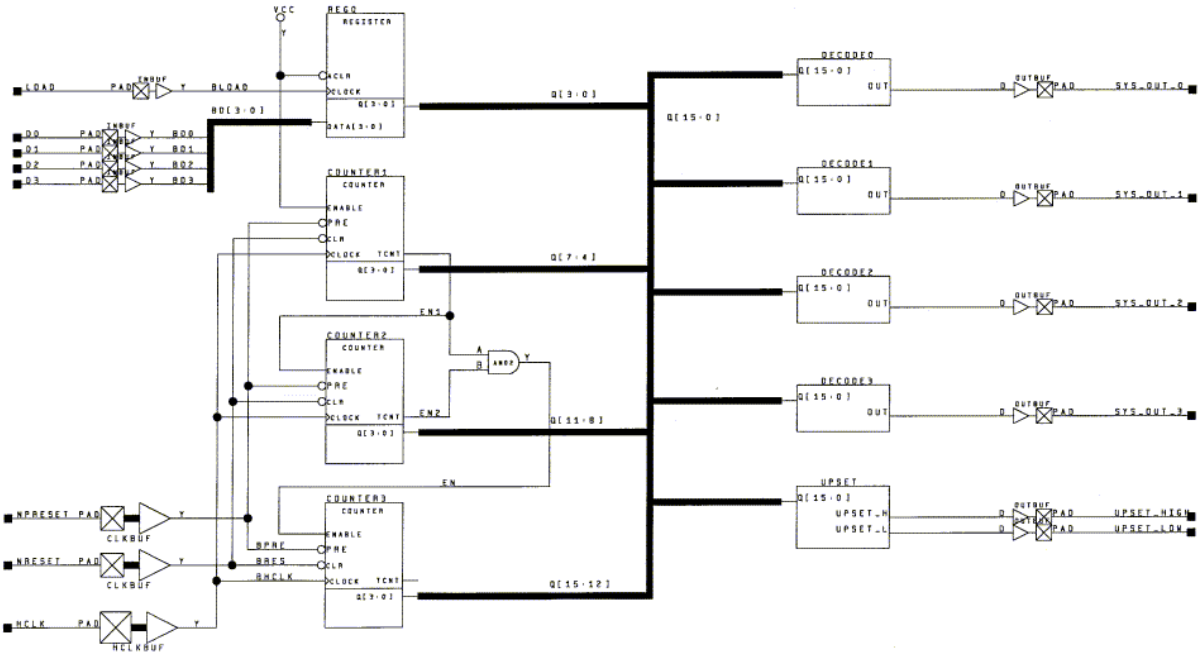

Figure 4.1. The FPGA test circuit

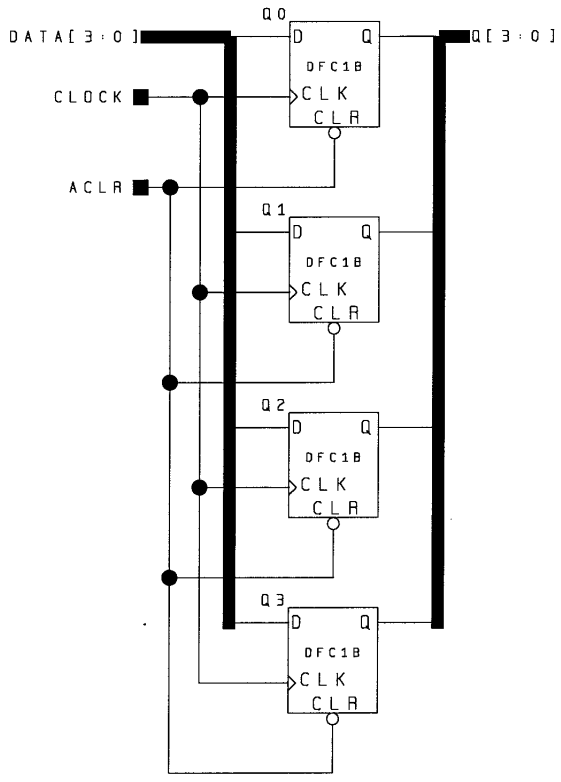

Figure 4.2. Implementation of REG0 in the FPGA circuit.

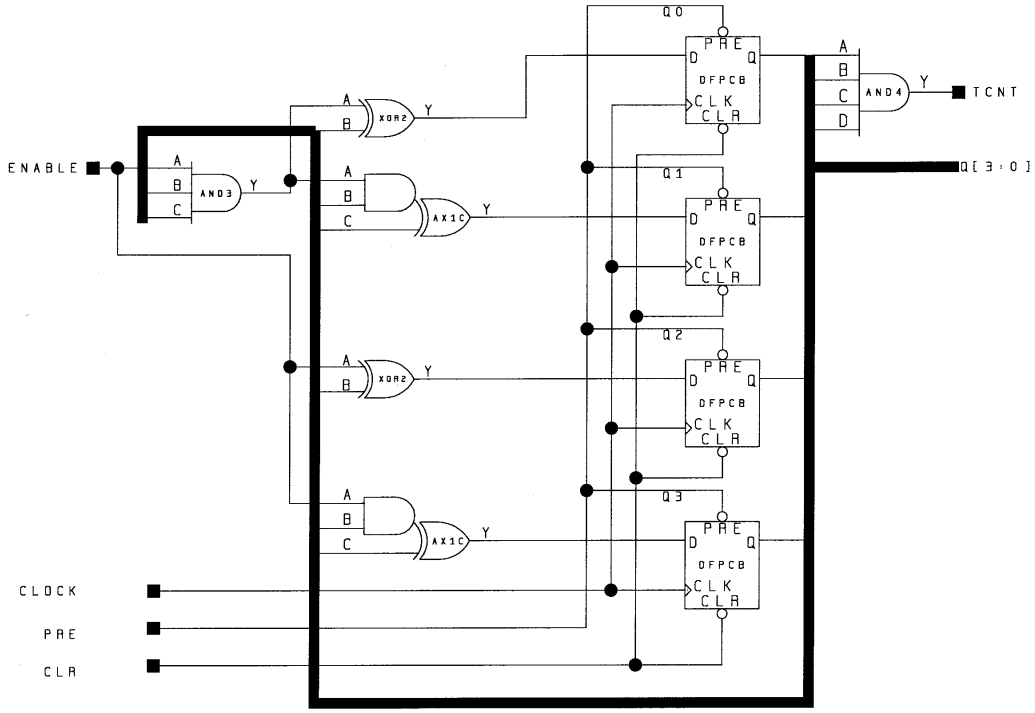

Figure 4.3. Implementation of the counters in the FPGA circuit.

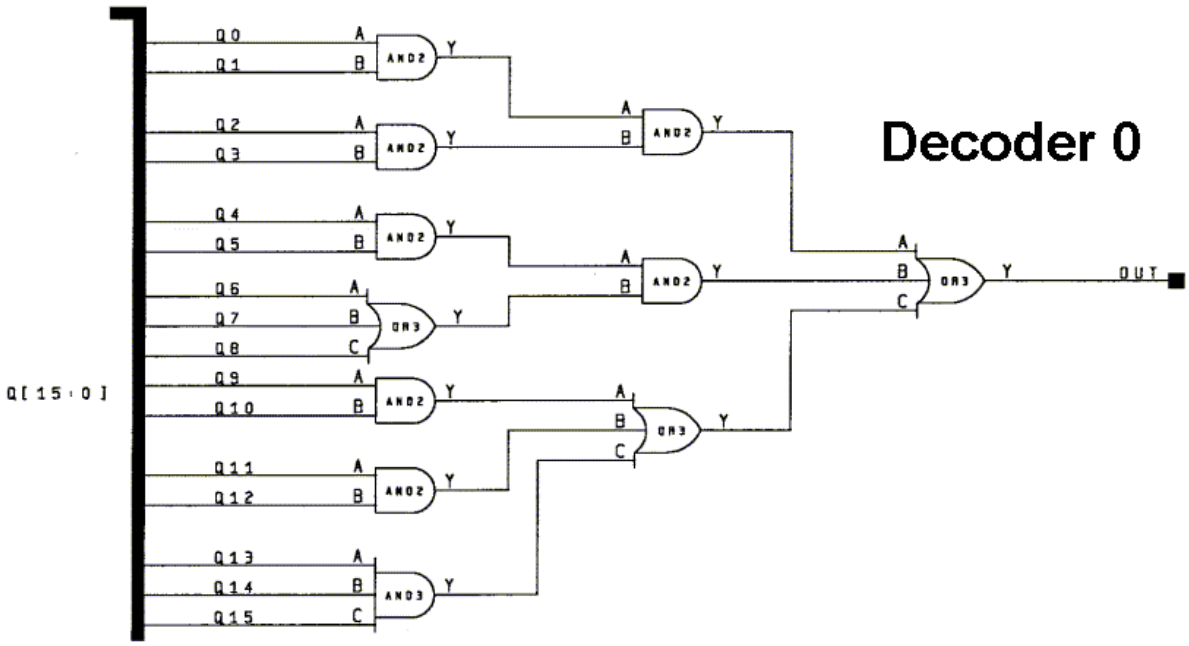

Figure 4.4. Decoder 0 logic in the FPGA circuit.

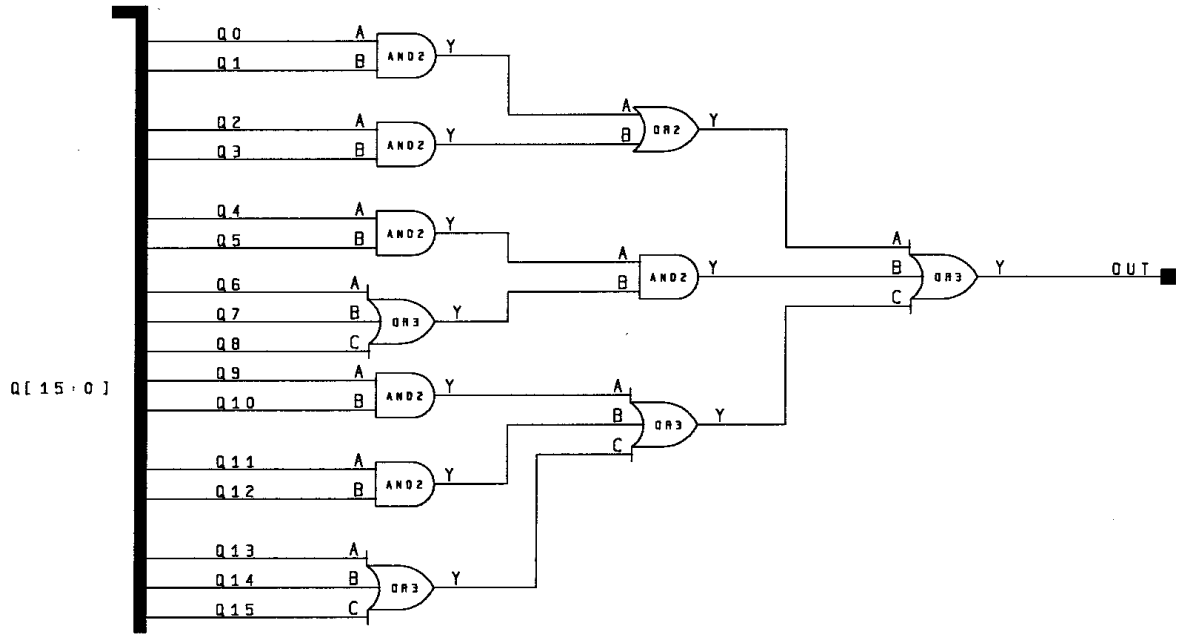

Figure 4.5. Decoder 1 logic in the FPGA circuit.

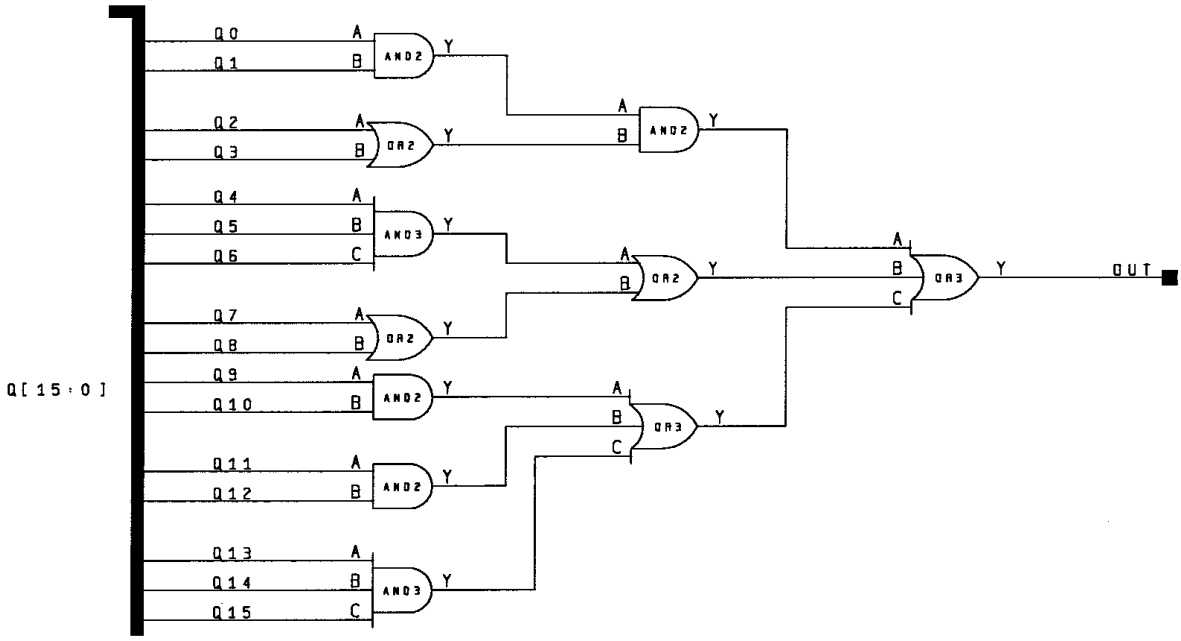

Figure 4.6. Decoder 2 logic in the FPGA circuit.

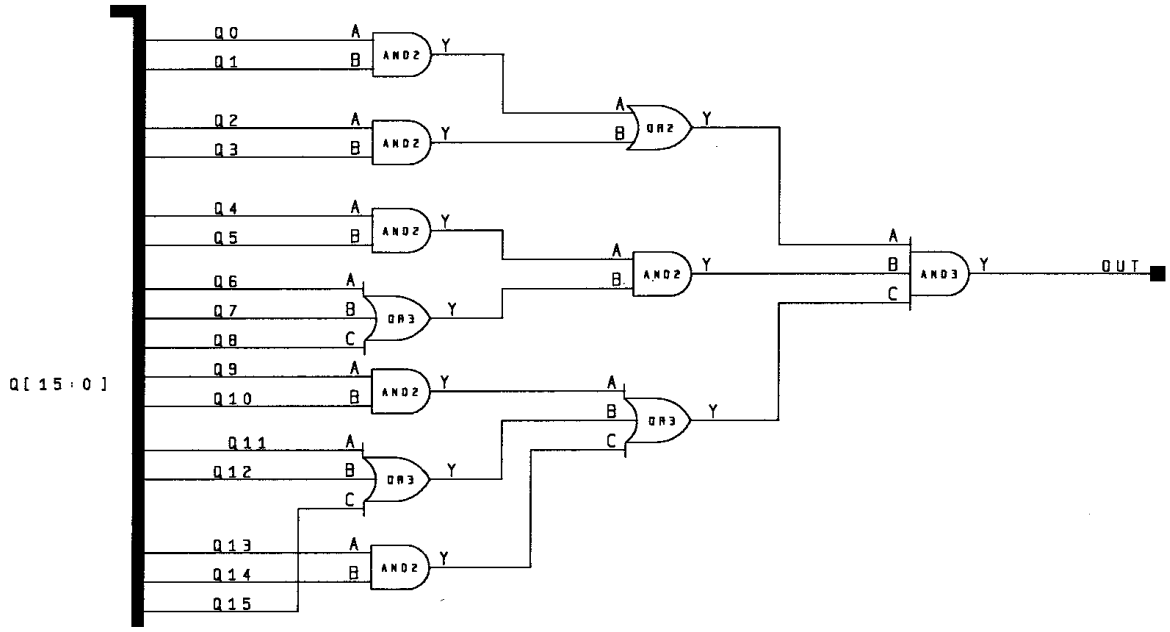

Figure 4.7. Decoder 3 logic in the FPGA circuit.

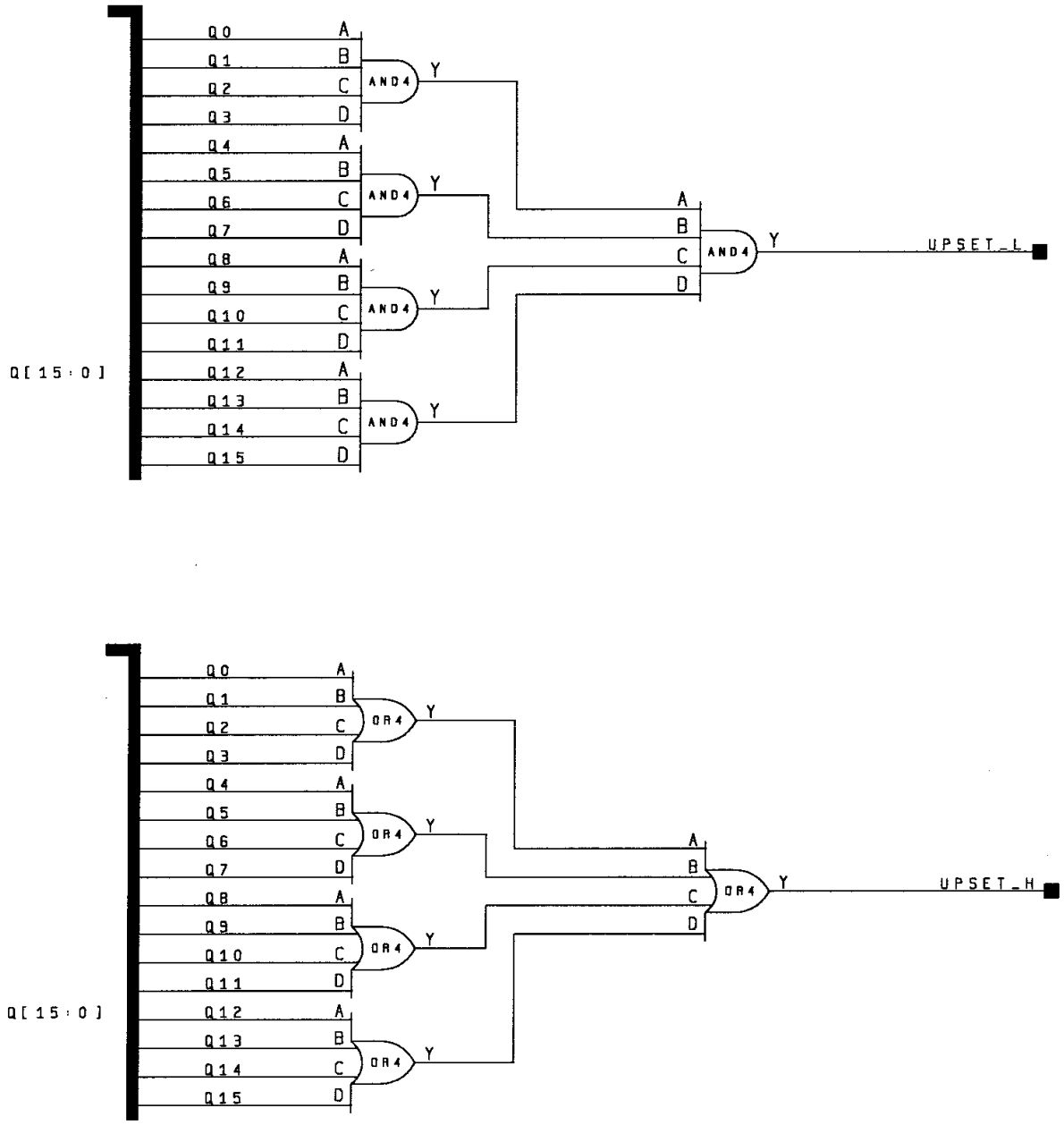

Figure 4.8. AND and OR generalised upset detectors in the FPGA circuit.

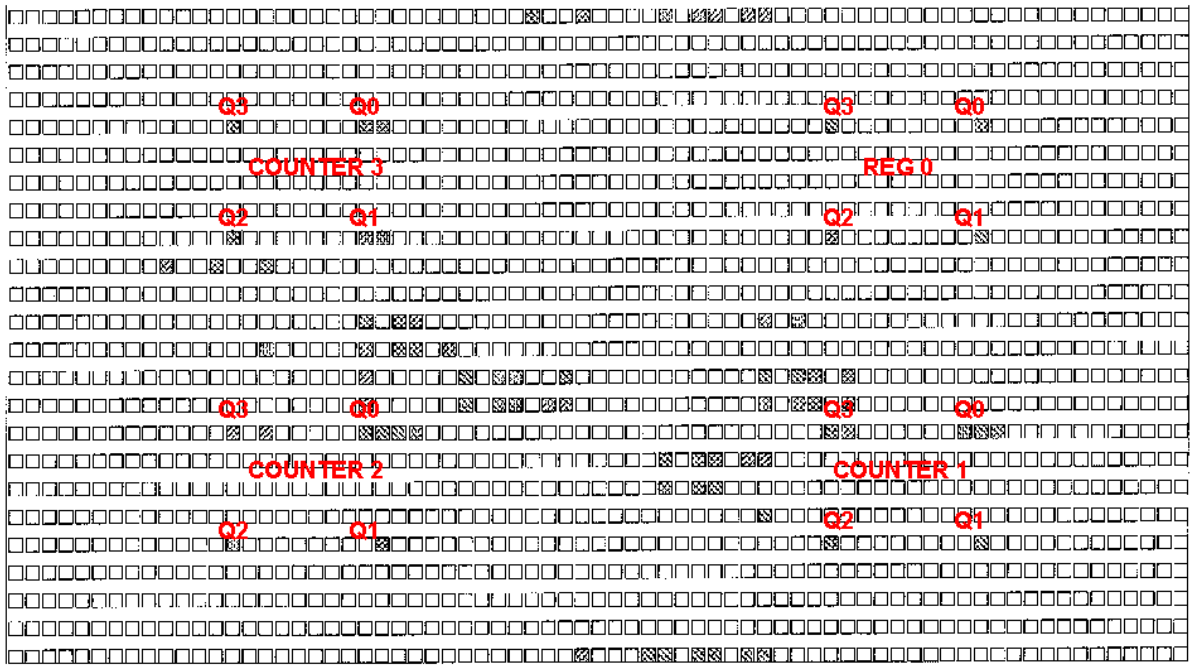

Figure 4.9. Map of the locations of the FPGA circuit elements on the device.

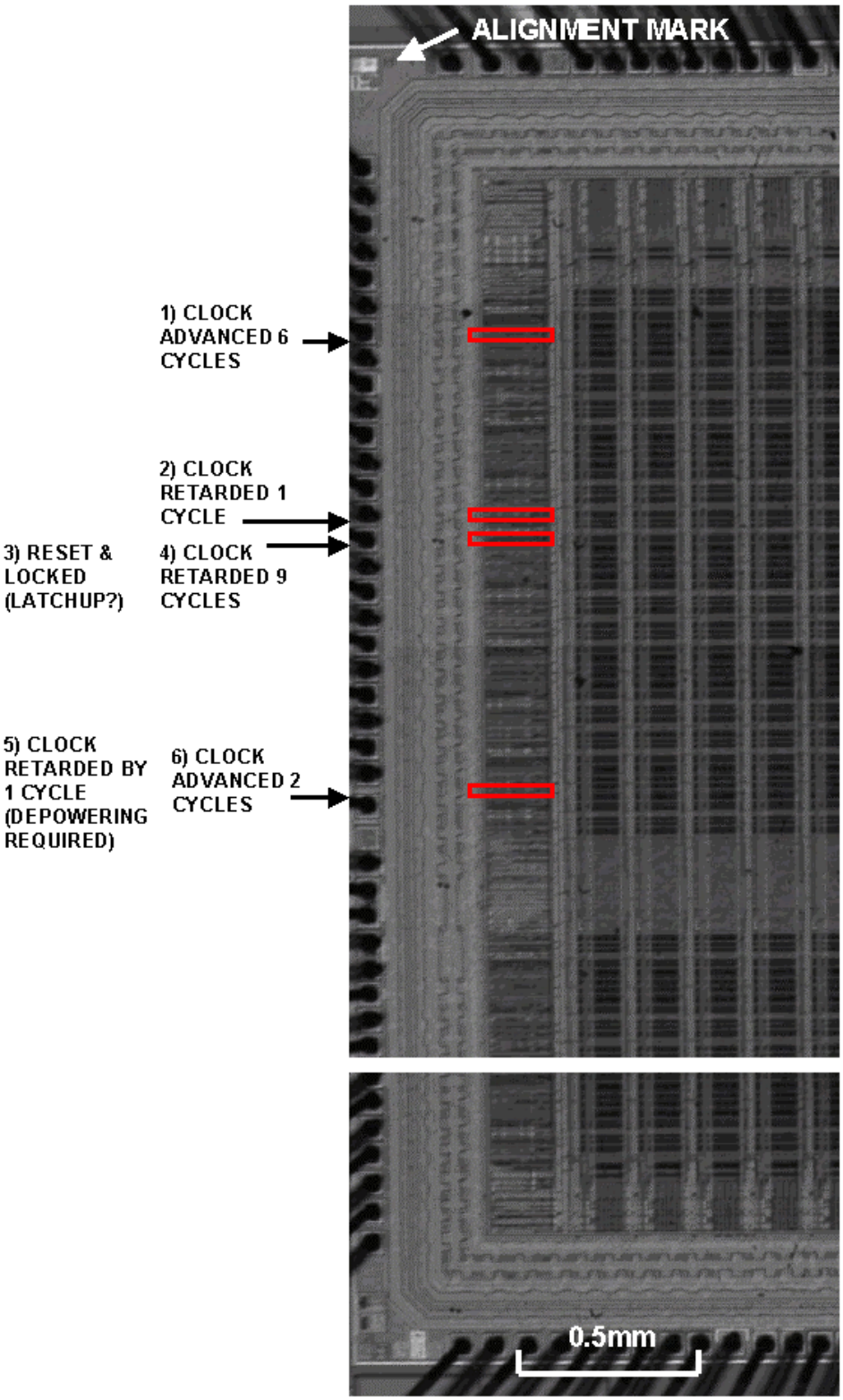

Figure 4.10. Laser induced errors observed in a strip down one side of the Actel 54SX16.

5.0 CONCLUSIONS AND RECOMMENDATIONS

5.1 Conclusions

5.1.1 The results of the two wavelength investigations of a range of 1Mbit SRAM's have shown that green pulses tend to give superior results to those obtained with infrared pulses. The trend of calibration coefficients (for relating laser pulse energy to equivalent ion testing LET's) with feature sizes is flat or slightly negative. This is particularly surprising for green pulses, since the calibration coefficient should theoretically be scaling in proportion to feature size, if the sensitive thickness of memory cells is scaling with feature size. The flatness of the observed trend suggests that the sensitive thicknesses are not scaling with feature size for these devices.

5.1.2 A laser method has been described and demonstrated, which measures the crucial sensitive volume parameters, that permit LET cross-section curves to be used to predict upset rates from proton and neutron fluxes. Since previous work (Ref. 3.1) has shown that the laser system can also be used to generate the LET cross-section curves, it potentially constitutes a self-contained apparatus for making fast and economical proton, neutron and ion SEE predictions for large numbers of device types. It offers the prospect of an excellent high volume and low cost screening system. However, regular calibration of a laser system against real radiation sources would be required to maintain confidence and accuracy.

5.1.3 It has also been shown that the laser technique is capable of being extended to measure the actual variations in the depthwise sensitivity profiles of microelectronic devices. This means that any problems with the technique due to the crudity of the sensitive volume approximation are addressable through a mere extension of the technique.

5.1.4 The ratios of the calibration coefficients for infrared and green pulses measured in these studies suggest that the sensitive thicknesses from all the devices are of the order of 10μm, which is significantly thicker than the well-thicknesses measured by NMRC. It would appear that significant charge is being gathered from the parts of the ionisation track within the substrate by the funnel effect. This probably explains why the green calibration coefficients do not scale with feature size.

5.1.5 The FPGA test results have succeeded in demonstrating the principle of linking output errors with corresponding sensitive die locations. However, the particular test device (Actel 54SX16) proved to be insensitive at many of the circuit components, which had been blown into it.

5.2 Recommendations

5.2.1 There are strong reasons to seek to add additional wavelength capabilities to the laser system. Notably, the conclusion that the sensitive thickness of memory cells may be static in the vicinity of 10 μm merits urgent validation and refinement. This work suggests that there should be particular interest in the wavelength range 600nm to 800nm (orange to near infrared). A planning study has suggested that the best means to achieve this aim is to introduce a Raman Tube in the 532nm laser beam path. This

would be capable of producing several wavelengths in the range 600nm to 700nm, depending on the gas species with which the tube were filled. The excellent wavelength and pulse energy stability of this type of system together with its low technical risk and economical costs make this approach preferable to any feasible continuously tuneable system. The capital cost of a Raman Tube will be borne by MBD internal funding and it is expected that the tube will be installed around September 2001. Funding for refined sensitive depth investigations with this new system is being sought.

5.2.2 This study has shown that there is a need to improve the monitoring of reflected laser pulse energy. This may be achieved by a careful extension of the current monitoring system, which relies upon a CCD camera viewing the focussed laser spot in the microscope image of the chip surface. The image needs to be captured into PC RAM with a video capture card, such that the illumination intensity in the pixels covered by the laser spot may be explicitly integrated. This should provide an excellent measure of pulse intensity, which may be compared with the pulse intensity similarly measured for a metal surface such as an area of metallisation (assumed to give virtually 100% reflectance) to establish the absolute reflectance on a pulse by pulse basis. This monitoring system could also provide a secondary method for calibrating the laser pulse energy.

5.2.3 The current SRAM studies should be repeated at the new laser wavelength(s) and detailed reflectance measurements should be undertaken for these devices.

5.2.4 The FPGA investigations should be repeated for more sensitive and more critical device types. A microprocessor with a known die map would be of particular interest.

REFERENCES

1.1 Francois-Xavier Guerre & Andrew Chugg, Utilisation of Pulsed Laser for SEE testing, Hirex-MBD Proposal No. HRX/99.4770, 16th September 1999.

3.1 Comparison Between SRAM Cross-Sections From Ion Beam Testing With Those Obtained Using A New Picosecond Pulsed Laser facility, R Jones, AM Chugg, CMS Jones, PH Duncan, CS Dyer & C Sanderson, IEEE Trans. Nuc. Sci., Vol. 47, No. 3, June 2000.

3.2 A New Approach for the Prediction of the Neutron-Induced SEU Rate, C Vial, JM Palau, J Gasiot, MC Calvet and S Fourtine, IEEE Trans. Nucl. Sci., Vol. 45, 2915-20, December 1998.

3.3 Microdosimetry Code Simulation of Charge-Deposition Spectra, Single Event Upsets and Multiple-Bit Upsets, CS Dyer, C Comber, PR Truscott, C Sanderson, C Underwood, M Oldfield, A Campbell, S Buchner and T Meehan, IEEE Trans. Nuc. Sci., Vol 46, 1486-93, December 1999.

3.4 Using A Carbon Beam As A Probe To Extract The Thickness Of Sensitive Volumes, C Inguimbert et al, IEEE Trans. Nuc. Sci., Vol. 47, No. 3, June 2000.

3.5 Constructional Analysis Report Number DTE1146, R Allison, T O'Shea, R Fitzgerald, NMRC, February 2001.

DISTRIBUTION

Recipient	Address	Copy numbers
A M Chugg	FPC005, Matra BAe Dynamics	1 - 2
Reno Harboe-Sorensen	ESTEC, Keplerlaan, Noordwijk, the Netherlands	3 - 5
Francois-Xavier Guerre	Hirex, Toulouse	6
Engineering Documentation Centre	Matra BAe Dynamics	7 & Master